Article

Origin of Podiform Chromitites in the Sebuku Island Ophiolite (South Kalimantan, Indonesia): Constraints from Chromite Composition and PGE Mineralogy

Arifudin Idrus [1] , **Federica Zaccarini** [2,*] , **Giorgio Garuti** [2] , **I Gusti Ngurah Kusuma Wijaya** [1] , **Yoseph Calasanctius Amita Swamidharma** [3] **and Christoph Bauer** [4]

[1]   Department of Geological Engineering, Universitas Gadjah Mada. Jl. Grafika 2 Bulaksumur, Yogyakarta 55281, Indonesia; arifidrus@ugm.ac.id (A.I.); kusumawijaya360@gmail.com (I.G.N.K.W.)
[2]   Physical and Geological Sciences, Faculty of Science, Universiti Brunei Darussalam, Jalan Tungku Link, Gadong, Bandar Seri Begawan BE1410, Brunei; giorgio.garuti1945@gmail.com
[3]   P.T. Sebuku Iron Lateritic Ore, Jalan Pluit Utara Raya No. 18 Jakarta, Kota Jkt Utara 14450, Indonesia; yoseph.swamidharma@yahoo.com
[4]   RHI Magnesita, Magnesitstrasse 2, A8700 Leoben, Austria; christoph.bauer@rhimagnesita.com
*   Correspondence: federicazaccarinigaruti@gmail.com; Tel.: +43-664-3868590

Abstract: The presence of PGM associated with the podiform chromitites in the Jurassic–Cretaceous ophiolite of Sebuku Island (South Kalimantan, Indonesia) is reported for the first time. Two types of chromitite have been recognized; one with high-Cr composition $(Cr/(Cr + Al) > 0.7)$ occurs in the deep mantle, the other, high-Al $(Cr/(Cr + Al) < 0.6)$, is located close to the Moho transition zone. The TiO_2-Al_2O_3 relations indicate affinity to IAT and MORB, for the high-Cr and high-Al chromitites, respectively. However, both are believed to have formed by mantle/melt reaction and differentiation of a magma characterized by an initial IAT composition related to an SSZ. Primary magmatic inclusions (<10 µm) of laurite characterized by Ru/Os chondritic ratio are the only PGM found in the high-Cr chromitites, indicating crystallization from undifferentiated magma, at low fS_2 in the mantle. In contrast, the high-Al to chondrite, suggesting the increase of fS_2 in the evolved melt. Besides laurite, the high-Al chromitite contains a complex assemblage of secondary PGM (Pt-Fe, garutiite, iridium, ruthenium–magnetite aggregates, zaccariniite and unnamed Ru and Mn oxides). These secondary PGM have an irregular shape and occur exclusively in the chlorite matrix sometimes associated with Mn-Ni-Fe-Cr hydroxides. They are interpreted to have formed by desulfuration of primary interstitial PGM sulfides or to have precipitated from secondary fluids during low T alteration. The relative abundance of PPGE in the high-Al chromitite is interpreted as a result of PGE fractionation during differentiation of the parent melt of the chromitites.

Keywords: chromitite; platinum group minerals; ophiolite; Sebuku Island; Borneo; Indonesia

1. Introduction

Chromitite is an economically important rock, because it is the only natural source for chromium recovery. Chromite, being relatively resistant to alteration, can be used as an important petrogenetic indicator [1–3]. For many decades, chromitite has been recognized as an efficient collector of the strategic platinum group elements (PGE = Os, Ir, Ru, Rh, Pt, Pd). Some chromitites are preferentially enriched in IPGE (IPGE = Os, Ir, Ru) and others are dominated by PPGE (PPGE = Rh, Pt, Pd), depending on the degree of the partial melting of the mantle source, PGE fractionation during crystallization of the parent melt, T and fS_2 [4]. Post-magmatic processes can also be responsible for various types of PGE enrichment in ophiolitic chromitites [5].

The PGE are mainly carried in tiny grains, generally less than 20 µm in size, of specific platinum group minerals (PGM). The PGM occur as inclusions in chromite grains. The

PGM could also occur in the silicate matrix and along cracks in chromite grains, which can further be opened or healed due to recrystallization processes. The PGM enclosed in fresh chromite are generally preserved by alteration and are referred to as primary PGM, having crystallized at high T during the magmatic stage [6–10]. On the contrary, the PGM not included in chromite are exposed to alteration and, in some cases, can be altered and reworked at a small scale by the action of low T fluids forming the so-called secondary PGM [5,8–15]. Two different types of chromitite have been described within the ophiolite complexes: (1) podiform chromitite that is typically hosted in the mantle tectonite and (2) stratiform chromitite occurring concordantly with the layered ultramafic rocks at the base of supra-Moho cumulates, above the crustal sequence [8,9]. According to Prichard et al. [9], the mantle-hosted podiform chromitite is high-Cr whereas the high-Al chromitite occurs at higher levels close to the Moho.

Most podiform chromitites show an enrichment of the IPGE over the PPGE, though a few exceptions have been reported. Selected exceptions include chromitites from Canada [10,16,17], from the Caribbean area [18–20], from north and central Europe [21–23], from the Balkan Peninsula [24–26], from Turkey and Saudi Arabia [8,9], from Eastern Sayan in Russia [14,27,28] and from the Philippines and New Caledonia [11,12,29]. The PPGE rich chromitites occur in the mantle and in the crustal sequence of the host ophiolite, regardless of the composition of the host chromite [10–29].

The first occurrence of PGM in the island of Borneo was documented in 1866, when laurite $(Ru,Os)S_2$, the most common Ru mineral, was discovered in a placer deposit located in the Riam Pinang area in South Kalimantan. Later, also the rare PGM vincentite $(Pd,Pt)_3(As,Sb,Te)$ was found in platinum–gold concentrates from the Riam Kanan River, in the Banjar Regency situated in South Kalimantan [30]. More recently, several authors confirmed the presence of abundant PGM nuggets, mostly composed of laurite and Pt-Fe alloys, collected in the Tambanio area, Pontyn and Kanan Rivers and derived by the erosion of ultramafic rocks related with the South Kalimantan Meratus–Bobaris ophiolite, and from the Edam River near the town of Lahad Datu, East Kalimantan [31–34]. On the contrary, Zientek et al. [35], on the basis of PGE geochemistry and mineralogy, observed that several placer deposits of South Kalimantan are very similar to those related with the Alaskan-type ultramafic complexes.

The occurrence of PGM, such as laurite and Ru-Os-Ir alloys associated with podiform chromitite lode deposits of Borneo, was documented only from the ultramafic rocks of the Meratus–Bobaris ophiolite located in the south portion of the Meratus Mountains, southeast of Kalimantan [36].

This contribution describes a newly discovered PGM occurrence associated with small chromitite bodies in the Sebuku Island of South Kalimantan (Figure 1A,B). Detailed studies by field emission scanning electron microscopy (FE-SEM) and electron microprobe analyses have revealed a complex assemblage of primary and secondary PGM, consisting of Os, Ir, Ru, Rh and Pt phases. The composition and the paragenesis of PGM and of the host chromite and associated silicates are used to discuss the genetic aspects of the mineralization and the evolution of the PGM from the magmatic stage down to lower T proper to hydrothermal and supergene alteration.
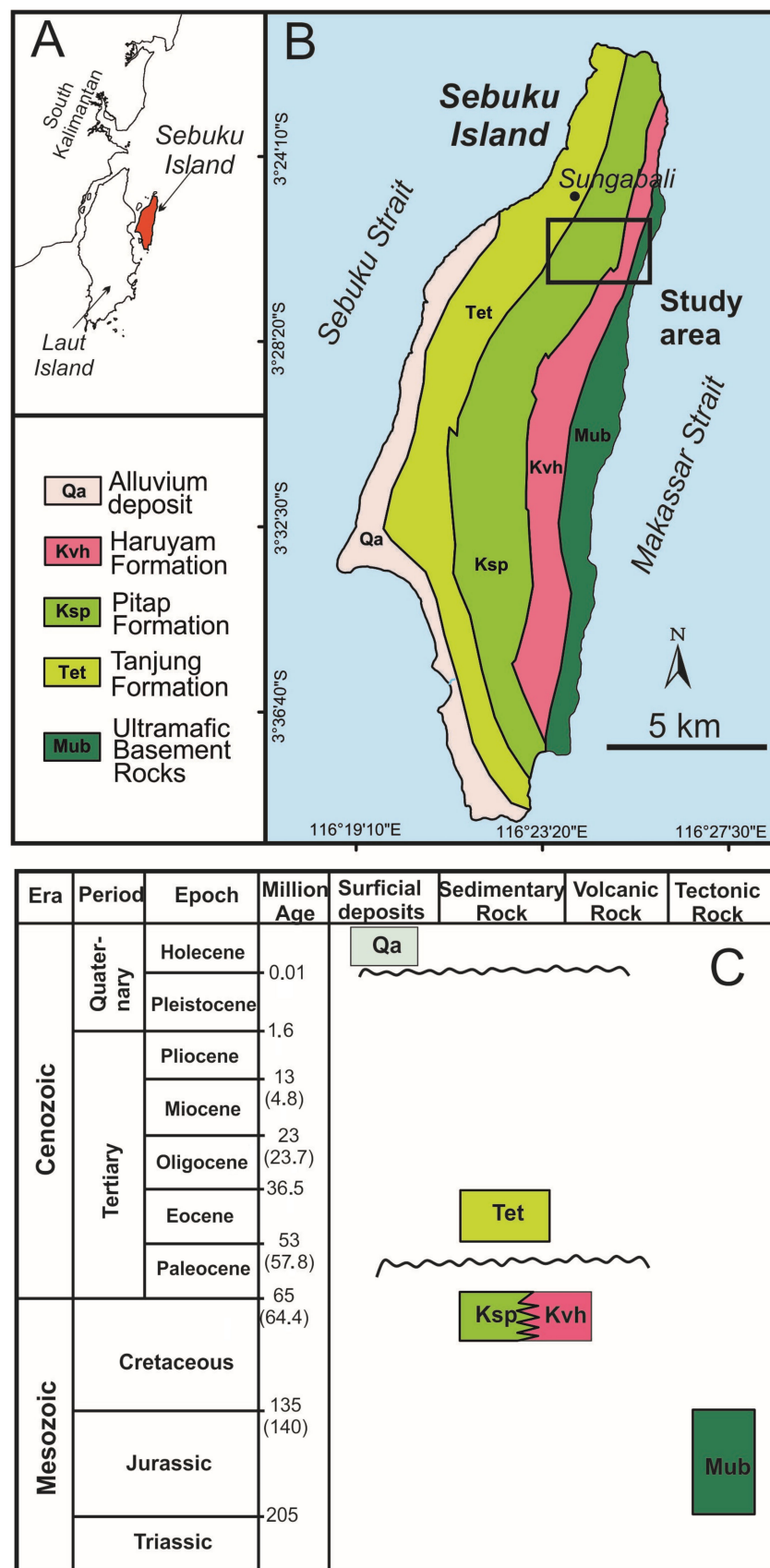
Figure 1. (**A**) Location of Sebuku Island in the SE corner of Borneo (Kalimantan) Island, (**B**) geological map of Sebuku Island (modified from Rustandi et al. [37]) showing the location of the study area and (**C**) regional stratigraphy of Sebuku Island (modified from Rustandi et al. [37]).

2. Regional Geology of Sebuku Island

Sebuku is a small island, about 10×30 km², located a few km east of the larger Laut Island, and lies between the Sebuku and the Makassar Straits in (Figure 1A,B). According to the Regional Geological Map of Kotabaru Sheet, South Kalimantan [37], Sebuku Island comprises the following rock formations, listed from the oldest to the youngest: Ultramafic Basement Rock (Mub), Pitap Formation (Ksp), Haruyan Formation (Kvh), Tanjung Formation (Tet) and Alluvium (Qa) (Figure 1B) as illustrated in the stratigraphic column of Figure 1C.

The Ultramafic Basement Rock (Mub) is the oldest formation estimated to be Jurassic in age (Figure 1C) and is composed of peridotites such as harzburgite and dunite partially altered or totally transformed in serpentinite. Fragments of gabbro, basalt and pyroxenite have been also recognized in the Mub, but it was not possible to establish their relationships with the ultramafic rocks.

The Pitap Formation is composed of conglomerate intercalated with wacke sandstone, interbedded sandstone and siltstone. It also consists of limestone, polymictic breccia, claystone, conglomerate and basalt. The conglomerate is characterized by well stratification with some fragments of basalt, claystone, ultramafic rocks, chert, limestone, gabbro and diabase. The formation is supposed to have been formed in the Late Cretaceous period (Figure 1C) in a shallow sea environment. The thickness of the formation ranges between 1000 and 1500 m and it was interfingered to the Haruyan Formation.

The Haruyan Formation is made up of pillow lava, polymictic breccia and tuff. The breccia is composed of basalt, chert, siltstone and greywacke fragments. The formation thickness is about 1250 m and it is interfingered to the Pitap Formation. According to Figure 1C, the estimated rock formation age is Late Cretaceous.

The Tanjung Formation is composed of intercalation of conglomerate, sandstone and claystone with minor shale, clay and limestone. The lower part of the formation comprises conglomerate and sandstone intercalated with claystone, shale and coal seams. The upper part of the formation consists of sandstone and claystone interbedded with limestone, which contains foraminifera fossils such as *Discocyclina* sp., *Nummulites* sp. and *Lepidocyclina* sp. The Tanjung Formation, about 1500 m in thickness, is estimated to have been deposited during the Eocene period during the transition of the fluvial to the upper deltaic environment. The formation unconformably overlies the Pitap and the Haruyan Formations. Alluvium deposit is composed of loose sediments of the fluvial, shore and swamp deposits, with particle sizes varying from pebbles, granules, sand, clay and mud.

Sebuku Island hosts a portion of the ophiolite overthrust which formed during the subduction of eastern Sulawesi during the Miocene–Pliocene period. The structural process formed the SW-NE fold-thrust belt system with several minor geologic structures such as strike-slip faults, thrust faults and folds [38].

3. Geology of the Studied Area and Description of the Sebuku Chromitites

The studied area, located southeast from the village of Sungabali (Figure 1B), is characterized by an undulating morphology and is strongly affected by weathering and supergene processes that generated a thick layer of altered soil hosting economic deposits of lateritic iron, presently mined by a private national company, PT. SILO. On the basis of field geological and petrographic observations, the following major rock units have been described: harzburgite and dunite partially altered at low T and pressure, serpentinite, microdiorite, altered sandstone and alluvium deposits [39] (Figure 2) and partially altered peridotites and serpentinite belong to the Ultramafic Basement Rocks [37].
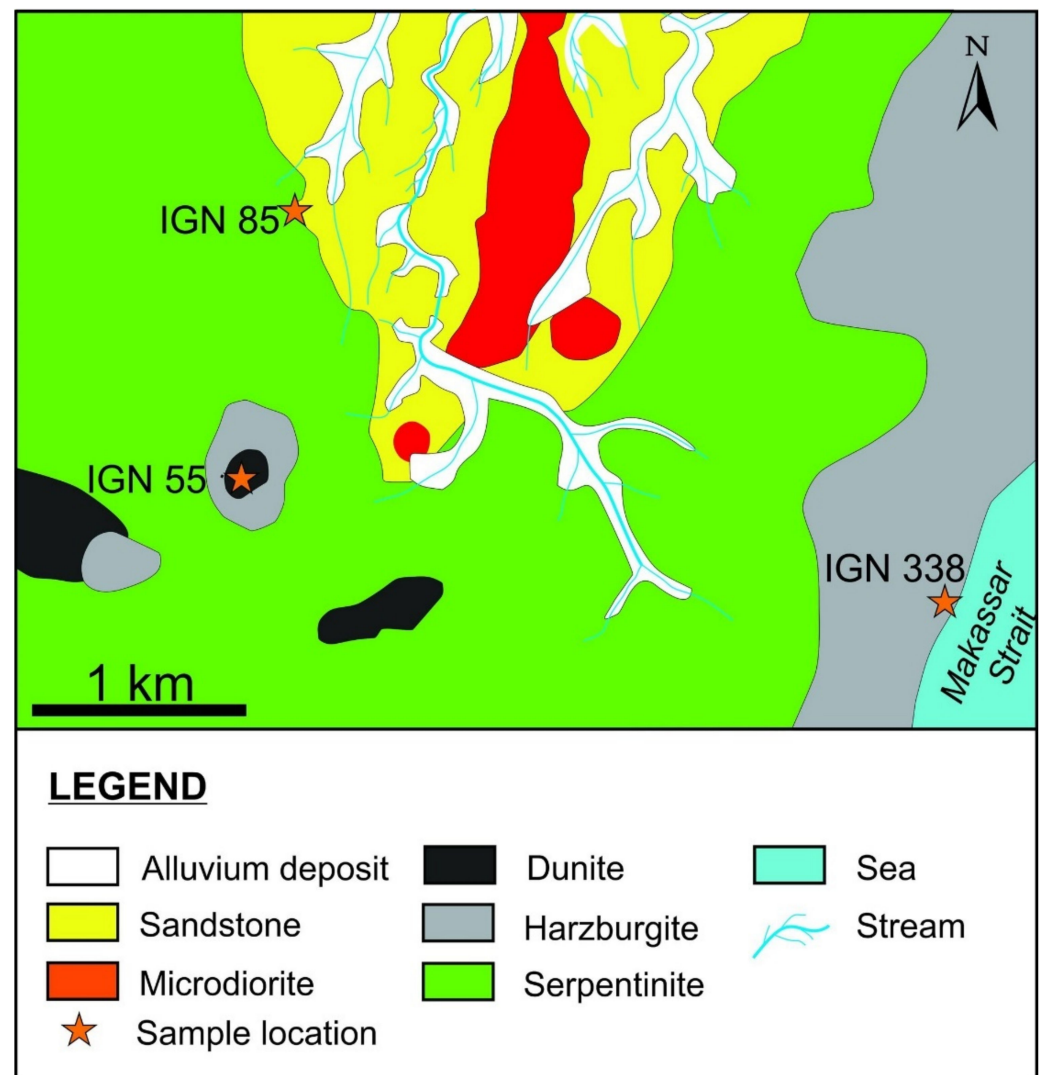
Figure 2. Geological map of the studied area showing the location of the chromitite hosted by ultramafic rocks in Sebuku Island (modified from Wijaya [39]).

Locally, small bodies of fresh harzburgite, dark grey in color but brownish when affected by weathering, have been found. Based on field and petrographic observations and despite the incipient alteration, two types of harzburgite have been recognized: (i) harzburgite representing an upper mantle tectonite which is characterized by a boudinage structure containing fragments of gabbro, altered dunite, altered lherzolite and podiform chromite that are distributed in the eastern portion of the study area, and (ii) harzburgite associated with altered dunite, altered lherzolite and silicified rocks that shows affinity with the ultramafic cumulates overlaying the mantle tectonite [39].

Dunite is generally moderately to strongly serpentinized and it occurs in the middle and southwestern part of the study area, with a longitudinal distribution in the northeast–southwest direction. It is generally covered by vegetation or lateritic soil and is reddish-brown to brown in color when altered (Figure 3A,B). Fresh dunite is rare and shows a dark green color. Small lenses of podiform chromitites occur in the partially altered dunite (Figure 3C–F).
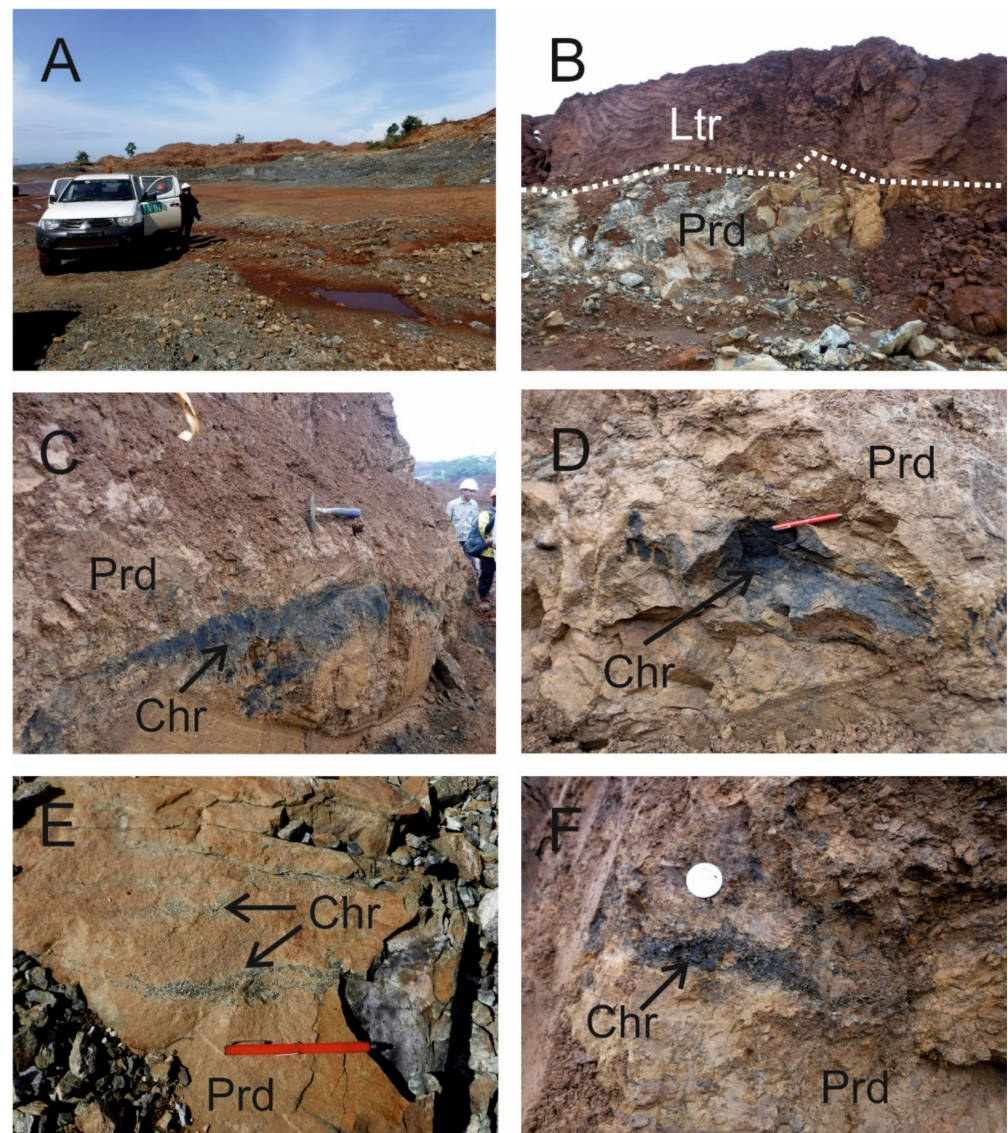
Figure 3. General overview of selected outcrops of the studied chromitites in Sebuku Island: (**A**) field image of weathered peridotite which hosts the chromitites, (**B**) lateritic horizon of bedrock peridotite, (**C**) schlieren of massive chromitite, (**D**) pod of massive chromitite, (**E**) thin layered and disseminated chromitites and (**F**) small pocket of massive chromitite within weathered peridotite. Abbreviations: Chr—chromitite, Lrt—laterite, Prd—weathered and altered peridotite.

Serpentinite is the most abundant rock in the study area. It is generally covered by vegetation or thick red and yellow limonite lateritic soil. Locally, serpentinite is silicified due to hydrothermal alteration [39].

Microdiorite crop outs in the middle north of the study area with a north–south longitudinal pattern. This unit corresponds to Upper Cretaceous diorite [37]. Microdiorite are in contact with metasandstone and alluvium deposits. The sandstone is part of the Pitap Formation and the Haruyan Formation which formed during the Upper Cretaceous [37] period. Alluvium deposits occur in the middle of the study area and are distributed along the stream. The unit consists of loose sediment and contains fragments of ultramafic rocks, gabbro and lateritic iron. Regionally, this unit corresponds to Holocene alluvium, as defined by Rustandi et al. [37].

The chromitite samples were collected in an area strongly affected by weathering and supergene processes that generated a thick layer of altered soil hosting economic deposits of lateritic iron, presently mined by PT. SILO. The studied chromitites represent

different types of chromite ore, varying from massive pod (sample IGN338) and schlieren (sample IGN55A) to disseminated with up to 50 vol% proportion of silicates (samples IGN55, IGN55C and IGN85). Sample IGN338 was collected in the southeast portion of the studied area and occurs in the altered harzburgite. Samples IGN55, IGN55A and IGN55C are hosted in a small altered dunite body, in contact with an altered harzburgite. Sample IGN85 occurs in the serpentinite, close to the contact with the sandstone (Figure 2).

4. Methods

Fourteen polished sections were previously studied by reflected-light microscopy to locate the minerals of interest. PGM, chromite and silicates were analyzed by electron microprobe using a Superprobe Jeol JXA 8200 installed at the Eugen F. Stumpfl Laboratory at the University of Leoben, Austria, using both energy dispersive (EDS) and wavelength dispersive (WDS) systems. Back-scattered electron (BSE) images were obtained using the same instrument.

Selected PGM, characterized by complex assemblages, were also investigated using a JEOL JSM-7900F field emission gun scanning electron microscope, in combination with an Oxford Xmax 80 silicon drift detector, available at RHI Magnesita Technology Center of Leoben, Austria. Acceleration voltage was 20 kV, working distance was 11 mm and probe current was 2 nA.

During the quantitative analyses of chromite and silicates, the electron microprobe was operated in the WDS mode, with an accelerating voltage of 15 kV and a beam current of 10 nA. The analyses of Na, Mg, K, Al, Si, Ca, Ti, V, Cr, Zn, Mn, Fe and Ni were obtained using the Kα lines and were calibrated on natural chromite, rhodonite, ilmenite, albite, pentlandite, wollastonite, kaersutite, sphalerite and synthetic metallic vanadium. The following diffracting crystals were selected: TAP for Na, Mg, Al; PETJ for K, Si, Ca; LIFH for Ti, V, Cr, Zn, Mn, Fe, Ni. The peak and background counting times were 20 and 10 s, respectively, for the major elements. They were increased to 40 and 20 s for the trace elements, such as Ca, Ni and Mn in olivine. The amount of Fe^{3+} in chromite was calculated assuming the spinel stoichiometry $R^{2+}O\ R^{3+}_2O_3$. The detection limits were automatically calculated by the microprobe software and they are listed in the following as ppm: Ca (50), Na, Mg, K, Fe, Mn, (100), Al, V, Ni (150), Cr, Zn (200), Si, Ti (250).

The PGM smaller than 5 microns were only qualitatively analyzed by EDS. The larger PGM were quantitatively analyzed in the WDS mode at a 20-kV accelerating voltage and a 10-nA beam current, with a beam diameter of about 1 micron. The peak and background counting times were 15 and 5 s, respectively. The Kα lines were used for O, S, As, Cu, Mn, Fe and Ni, Lα for Ir, Ru, Rh, Pd and Pt and Mα for Os. The reference materials were pure metals for the six PGE (Ru, Rh, Pd, Os, Ir, Pt), synthetic NiS, magnetite for O, natural pyrite, chalcopyrite, rhodonite and niccolite for Ni, Fe, Cu, Mn, S and As. The following diffracting crystals were selected: LDE1 for O; PETJ for S; PETH for Ru, Os, Rh; LIFH for Cu, Mn, Fe, Ni, Ir, Pt; TAP for As. Automatic corrections were performed for interferences involving Ru-Rh and Rh-Pd. The calculated detection limits, in ppm, are: O, S, As (100), Fe, Ni, Cu, Mn (150), Rh, Pd, Ru (250), Os, Ir, Pt (350). The same instrument and conditions were used to obtain the elemental distribution maps.

5. Results

5.1. Texture and Composition of Chromite and Associated Silicates

Confirming the optical observation reported by Imani et al. [40], microscopically the chromitites of Sebuku Island display a texture variable from massive to highly disseminated with the interstitial silicates reaching a maximum modal proportion of 50% (Figure 4A–F). The massive samples locally show linear shear zones (Figure 4A) and brecciated texture (Figure 4B). Disseminated chromite consists of chromite, up to 1 mm in size, with lobate boundaries (Figure 4E,F). Chromite is cut by cracks filled with interstitial silicates, mainly composed of serpentine and chlorite (Figure 4A–F). Chromite is unaltered and rarely displays the development of very thin rim of ferrian chromite in few crystals (Figure 4E).
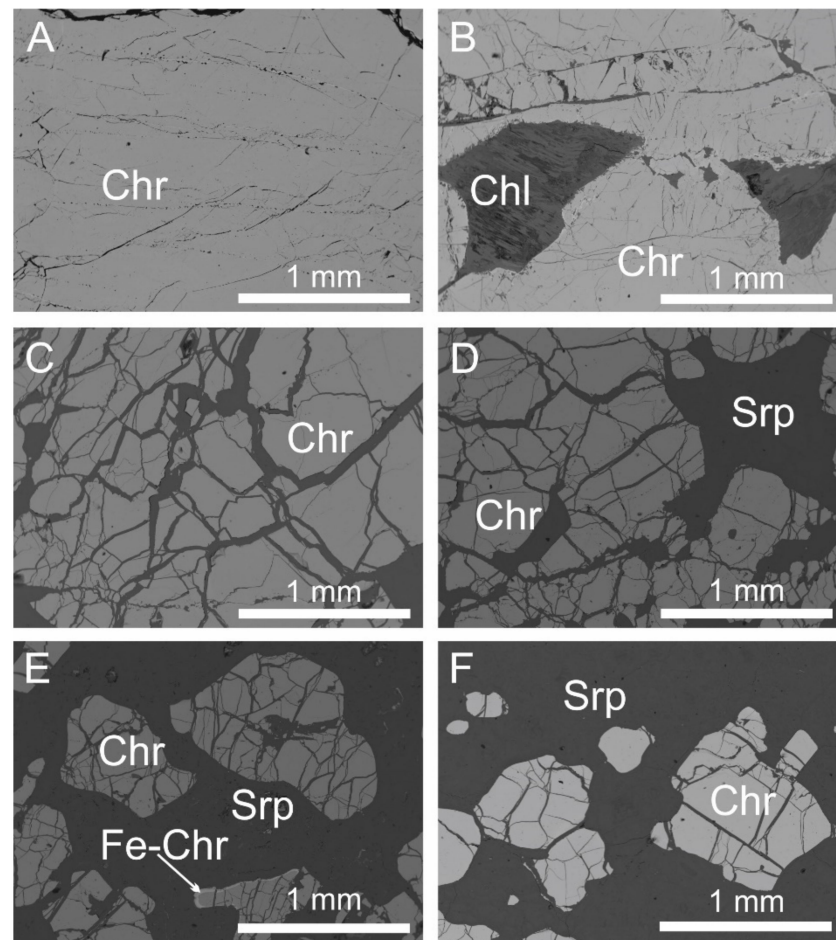
Figure 4. Back-scattered electron (BSE) images of polished sections from the Sebuku chromitites, showing massive (**A**) and partially brecciated chromite (**B**), fractured chromite (**C,D**) and massive chromite with about 40% of altered silicates (**E,F**). Few chromite grains show a thin rim of ferrian chromite (**E**). The altered silicates consist of serpentine and chlorite. Abbreviations: Chr—chromite, Chl—chlorite, Srp—serpentine, Fe-Chr—ferrian chromite.

Selected analyses of fresh chromite grains are listed in Table 1 and plotted in the diagrams commonly used to distinguish compositions of chromitites associated with ophiolite, layered intrusions and the Alaskan-type complex (Figure 5A–E).

Table 1. Average composition of chromite based on 30 points analyses (wt%) in the High-Cr and High-Al Chromitite of Sebuku Island.

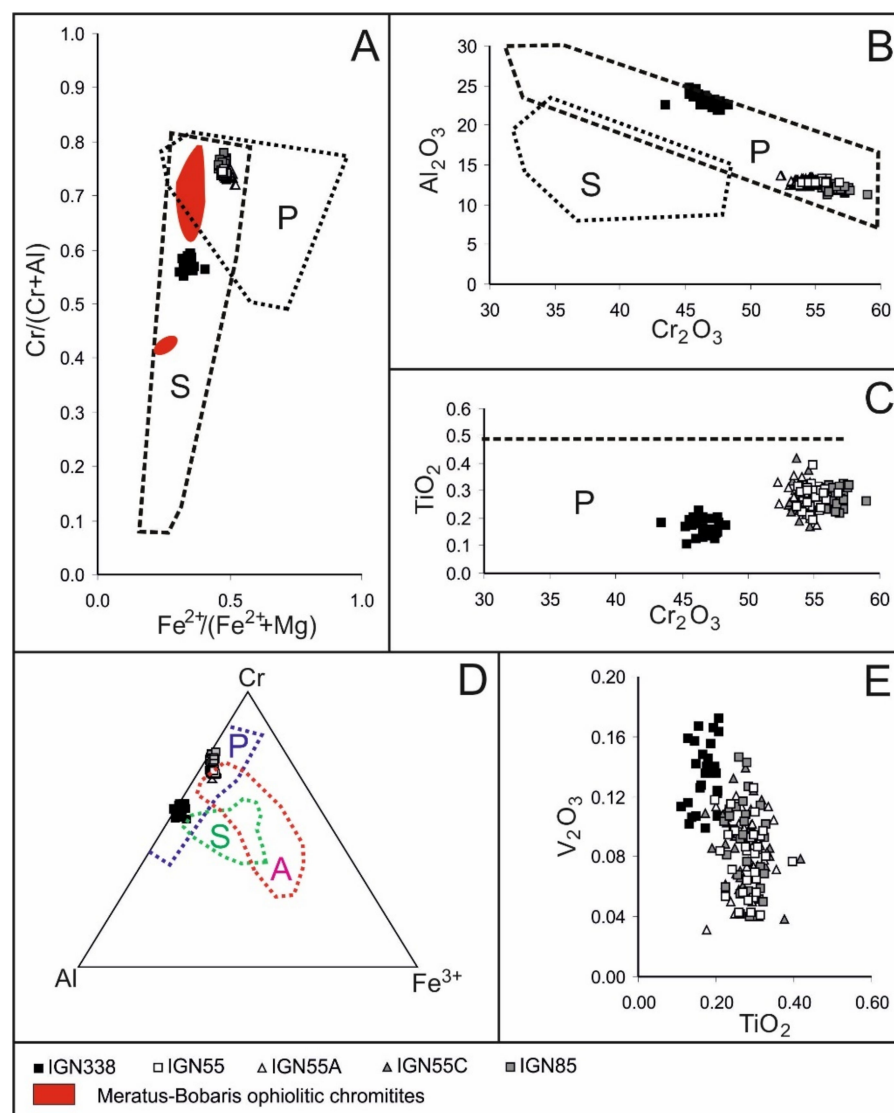| Cr# = Cr/(Cr + Al), Fe^{2+}# = (Fe^{2+}/Fe^{2+} + Mg).													
Sample	SiO$_2$	Cr$_2$O$_3$	Al$_2$O$_3$	TiO$_2$	FeO	Fe$_2$O$_3$	MgO	MnO	NiO	ZnO	V$_2$O$_3$	Total	Cr#	Fe^{2+}#
High-Cr chromitite														
IGN55c2	0.04	54.10	12.62	0.27	18.01	4.45	10.49	0.33	0.03	0.01	0.09	100.44	0.74	0.49
IGN55a2	0.04	54.22	13.10	0.28	18.32	3.72	10.36	0.32	0.05	0.02	0.08	100.50	0.74	0.50
IGN851	0.09	56.76	11.93	0.28	17.44	2.65	10.86	0.32	0.05	0.01	0.09	100.47	0.76	0.47
IGN5521	0.04	54.97	12.93	0.28	17.77	3.81	10.83	0.31	0.05	0.01	0.08	101.09	0.74	0.48
High-Al chromitite														
IGN338	0.06	46.55	23.12	0.17	13.42	1.48	14.43	0.21	0.12	0.01	0.13	99.70	0.57	0.34

Figure 5. Composition of unaltered chromite from the Sebuku chromitites showing the co-existence of high-Al and high-Cr chromitites: (**A**) variation of the chromium number, Cr# = Cr/(Cr + Al) and bivalent iron number, Fe^{2+}# = Fe^{2+}/(Fe^{2+} + Mg) and comparison with the chromitites from the Meratus–Bobaris ophiolite [36], (**B**) correlation between Al_2O_3 and Cr_2O_3, (**C**) variation of Cr_2O_3 and TiO_2, (**D**) Cr–Al–Fe^{3+} atomic ratios and (**E**) correlation of TiO_2 versus V_2O_3. *p*—field of podiform chromitites, S—field of stratiform chromitites, A—Alaskan-type chromitites [2,3,41–43].

In general, the Sebuku composition plots in the podiform field (Figure 5A–D) and the two main groups of chromitite have been recognized, such as high-Cr with Cr#, i.e., Cr/(Cr + Al), higher than 0.7 and high-Al with Cr# lower than 0.6 (Figure 5A), similarly to the chromitites from the Meratus–Bobaris ophiolite [35]. However, the chromitites from Meratus–Bobaris are characterized by lower Cr#and Fe^{2+}#, i.e., Fe^{2+}/(Fe^{2+} + Mg), compared with those of Sebuku. The Cr# varies from 0.72 to 0.78 in the high-Cr chromitite and from 0.55 to 0.59 in the high-Al chromitite. The Mg#, i.e., Mg/(Mg + Fe^{2+}), is comprised between 0.48 and 0.55 and 0.61 and 0.69 in the high-Cr and high-Al chromitites, respectively. Both the high-Cr and high-Al chromitites of Sebuku Island show a negative correlation between Cr_2O_3 and Al_2O_3 (Figure 5B), consistently with the Al-Cr substitution as observed in the podiform chromitites [39]. The affinity between the studied samples and the podiform chromitites is also confirmed by their low amounts of TiO_2 and Fe^{3+} (Figure 5C,D) [41–43]. The content of V_2O_3 is lower than 0.18 wt% in all the analyzed samples, although the high-Al chromitites are weakly enriched compared with the high-Cr (Figure 5E).

The binary diagrams of TiO_2 versus Al_2O_3, (Figure 6A,B) show that all the high-Cr chromitites fall in the field of the Island Arc Tholeiite (IAT) and the Supra Subduction Zone (SSZ) proposed by Kamenetsky et al. [44]. The high-Al chromitites display compositional similarities with those reported from the chromitites in the supra-Moho cumulate sequences of the Urals and Sulawesi ophiolite [45,46] and in the overlapping fields of the SSZ and the Middle Oceanic Ridge Basalt (MORB) chromitites. Similar compositions have been recently reported in the chromitites from Kabaena Island, Sulawesi [47].
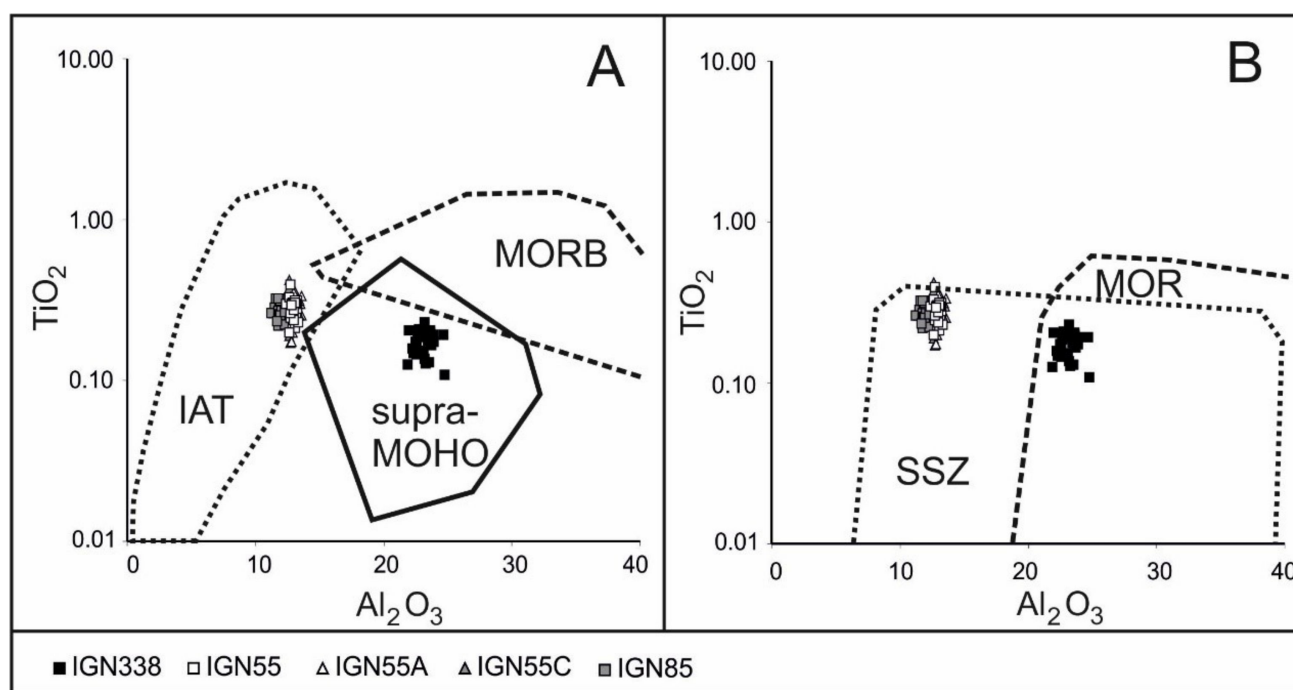

Figure 6. TiO_2–Al_2O_3 relationships in chromitites of Sebuku Island. (**A**) composition of the studied chromite, compared with the field of spinels from IAT, MORB mantle peridotites and supra-Moho cumulates (compositional fields from Kamenetsky et al. [44]; Garuti et al. [45]; Zaccarini et al. [46], (**B**) plot of chromite analyses, in comparison with the compositional fields of spinels from SSZ and MOR [44].

The calculated composition of the parental melt of the Sebuku Island chromitites, using as a tool the composition of chromite and based on the equations proposed by [48,49], shows that the Al_2O_3 varies from 11.89 to 12.31 in the high-Al and is 15.14 in the high-Cr chromitites. The TiO_2 is 0.4 in the high-Cr and 0.53 in the high-Al chromitites. These calculated values are in agreement with the composition of the chromitite that suggests an origin of the high-Cr and high-Al chromitites of Sebuku Island in equilibrium with melts related with an Arc and a MOR setting, respectively. Silicates in the matrix are completely altered to serpentine and chlorite silicates. Serpentine is the predominant silicate in the matrix of the high-Cr chromitites. Representative analyses listed in Table 2 show that analyzed serpentine is not homogeneous, with SiO_2 and MgO contents comprised between 38.26–45.92 wt% and 36.87–39.99 wt%, respectively. It is enriched in FeO, up to 4.98 wt%, and in NiO, up to 0.93 wt%. The other analyzed elements have been detected in concentration varying from below to close to the electron probe detection limit (Table 2). Microprobe totals are comprised between 82.97 and 89.49 wt%, falling in some cases below ideal for serpentine as also previously reported by Evans et al. [50] in serpentine from peridotite of the Duluth complex, USA.

Table 2. Representative analyses of serpentine (wt%) in the high-Cr chromitite of Sebuku Island.

| n.d.—Not Detected. | | | | | | | | | | | |
Sample	SiO$_2$	TiO$_2$	Al$_2$O$_3$	FeO	MnO	MgO	CaO	Na$_2$O	K$_2$O	Cr$_2$O$_3$	NiO	Total
IGN55-1	40.47	0.03	n.d.	4.21	n.d.	38.61	0.01	0.02	0.01	n.d.	0.48	83.84
IGN55-2	45.54	0.03	0.07	4.38	n.d.	37.70	0.02	0.02	n.d.	0.03	0.36	88.19
IGN55-3	39.88	0.02	0.04	4.52	n.d.	38.12	0.02	0.01	n.d.	0.01	0.54	83.19
IGN55-4	42.13	0.01	0.05	3.64	0.03	38.24	0.01	n.d.	n.d.	0.03	0.57	84.71
IGN55-5	45.18	n.d.	0.04	4.43	n.d.	39.31	0.04	0.02	n.d.	0.01	0.44	89.53
IGN85-1	45.92	n.d.	0.05	4.72	n.d.	37.02	0.02	n.d.	n.d.	0.04	0.93	88.70
IGN85-2	45.21	0.01	0.04	4.62	0.01	36.87	0.01	n.d.	n.d.	0.03	0.84	87.63
IGN85-3	45.89	0.01	0.02	3.70	n.d.	37.58	0.01	0.03	0.01	0.05	0.78	88.08
IGN85-4	43.87	n.d.	0.03	3.15	0.03	38.17	0.01	0.02	n.d.	n.d.	0.38	85.65
IGN85-5	44.12	n.d.	0.02	4.60	0.01	37.44	0.02	n.d.	0.01	n.d.	0.19	86.42
IGN55c-1	39.21	n.d.	0.01	3.67	0.06	39.99	0.02	n.d.	n.d.	n.d.	0.19	83.14
IGN55c-2	38.26	n.d.	0.03	4.98	0.12	39.04	0.03	0.01	0.01	n.d.	0.47	82.97
IGN55c-3	45.16	n.d.	0.07	2.99	0.04	39.23	0.02	n.d.	n.d.	0.04	0.69	88.26
IGN55c-4	43.73	0.03	0.01	3.52	0.04	38.64	0.01	0.01	n.d.	n.d.	0.38	86.40
IGN55c-5	45.21	n.d.	0.01	3.87	0.00	39.46	0.02	n.d.	0.01	0.05	0.88	89.49

Chlorite is the most abundant interstitial silicate in the high-Al chromitite and can be classified as clinochlore. The application of the chlorite geothermometer based on the amount of IVAl substituting for Si in the tetrahedral site [51] indicates that the chlorite crystallized in the thermal range of 230–274 °C (Table 3).

Table 3. Representative analyses of chlorite (wt%) associated with the high-Al chromitite of Sebuku Island.

| T °C Calculated Using the Geothermometer of Kranidiotis and McLean [49], n.d.—Not Detected. | | | | | | | | | | | | |
Sample	SiO$_2$	TiO$_2$	Al$_2$O$_3$	FeO	MnO	MgO	CaO	Na$_2$O	K$_2$O	Cr$_2$O$_3$	Total	T °C
IGN338-1	31.54	n.d.	16.60	1.39	0.02	33.21	0.03	0.06	0.02	3.07	85.93	230
IGN338-2	30.75	0.02	18.62	0.79	0.03	31.15	0.03	0.01	n.d.	3.49	84.88	241
IGN338-3	30.83	0.04	18.79	0.79	0.01	31.25	0.02	0.06	0.02	3.71	85.51	243
IGN338-4	31.50	0.09	19.66	0.81	0.00	32.40	0.05	0.06	0.02	2.98	87.56	246
IGN338-5	30.78	0.03	18.78	0.86	n.d.	32.08	0.04	0.01	n.d.	3.38	85.95	247
IGN338-6	31.33	0.03	19.22	1.75	n.d.	31.79	0.03	0.02	0.01	3.64	87.81	248
IGN338-7	30.37	0.10	19.51	0.91	n.d.	31.38	0.05	0.05	0.03	2.64	85.03	250
IGN338-8	30.44	0.11	19.45	0.95	n.d.	31.59	0.03	0.02	0.02	3.04	85.63	252
IGN338-9	30.97	0.08	19.52	0.96	0.02	32.49	0.02	0.01	n.d.	3.23	87.28	253
IGN338-10	30.60	0.07	18.98	0.90	0.02	32.44	0.01	0.03	0.01	3.39	86.45	254
IGN338-11	30.12	0.08	19.66	1.03	0.03	31.47	0.04	0.03	n.d.	2.51	84.96	255
IGN338-12	30.60	0.06	20.30	0.96	n.d.	31.62	0.08	0.04	0.03	2.89	86.58	256
IGN338-13	30.63	0.11	20.37	0.93	n.d.	31.81	0.03	0.02	n.d.	2.75	86.64	257
IGN338-14	30.66	0.09	20.67	1.02	0.08	31.89	0.05	0.01	0.01	2.37	86.83	258
IGN338-15	29.36	n.d.	13.64	1.10	0.02	31.61	0.01	0.07	n.d.	10.28	86.09	259
IGN338-16	29.83	0.01	19.74	0.99	0.05	31.72	0.03	0.04	n.d.	2.79	85.19	261
IGN338-17	30.47	0.08	21.16	1.02	n.d.	31.42	0.04	0.04	n.d.	2.74	86.96	262
IGN338-18	30.73	0.10	20.88	0.93	0.01	32.33	0.02	0.00	0.02	2.88	87.89	263
IGN338-19	30.23	0.14	20.35	1.09	0.00	32.05	0.02	0.03	n.d.	2.90	86.81	264
IGN338-20	30.20	0.05	20.73	0.71	0.03	31.65	0.04	0.04	n.d.	3.33	86.78	265
IGN338-21	30.57	0.12	21.28	0.95	n.d.	31.99	0.01	0.02	n.d.	2.83	87.76	266
IGN338-22	30.65	0.10	21.72	0.94	n.d.	31.90	0.04	0.01	n.d.	2.85	88.21	267
IGN338-23	30.51	0.12	21.42	0.95	0.06	32.20	0.01	0.01	n.d.	2.66	87.94	268
IGN338-24	30.53	0.11	21.61	0.92	n.d.	32.16	0.03	0.02	n.d.	2.79	88.16	269
IGN338-25	30.75	0.08	22.52	0.95	n.d.	31.84	0.06	0.02	n.d.	2.59	88.80	270
IGN338-26	30.24	0.11	21.61	0.93	0.02	31.93	0.02	0.04	n.d.	2.83	87.71	271
IGN338-27	29.88	0.02	20.74	0.99	0.01	32.15	0.04	0.06	0.01	3.11	87.01	272
IGN338-28	30.50	0.08	22.23	0.98	n.d.	32.22	0.01	0.03	0.01	2.76	88.82	274

Rare polygonal inclusions of olivine (20–60 μm) occur in chromite grains of the high-Cr chromitite (Figure 7A,B), representing the only relic of magmatic silicate.
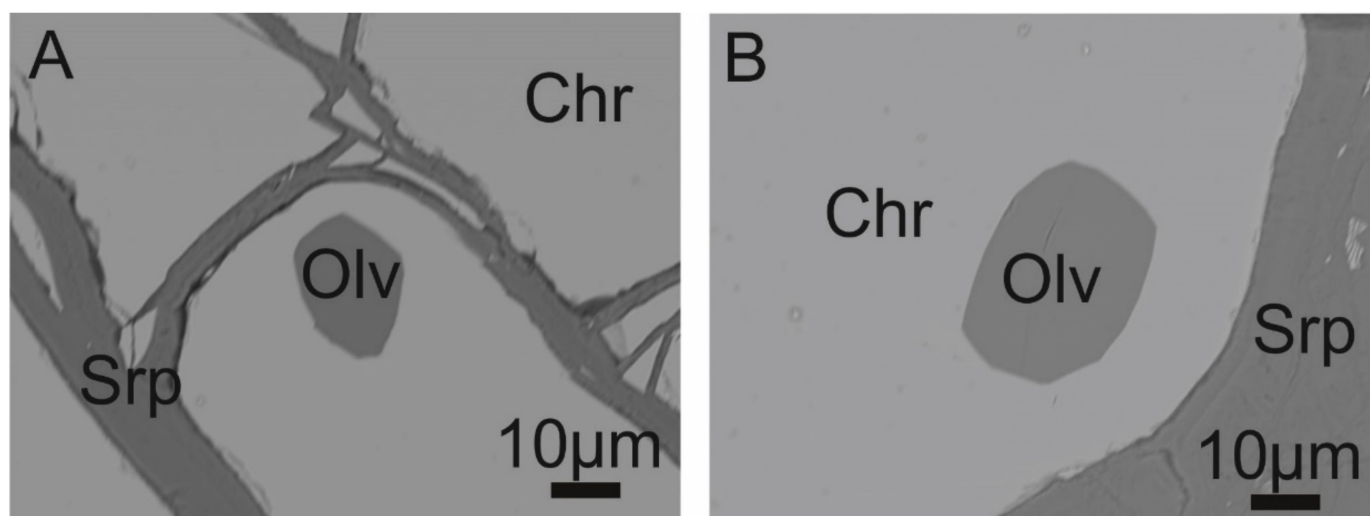

Figure 7. BSE images of olivine enclosed in high-Cr chromite and serpentine found in the matrix of the Sebuku Island chromitite (**A**,**B**). Abbreviations: Olv—olivine, Chr—chromite, Srp—serpentine.

Olivine displays a narrow range of the forsterite end member (Table 4) as typical of olivine associated with chromitite hosted in the ophiolitic mantle tectonite (Figure 8A–C). The NiO is very low compared with those of the olivine associated with ophiolitic chromitites and plots in the field of the Alaskan-type chromitites (Figure 8A).

Table 4. Representative analyses of olivine (wt%) included in the high-Cr chromitite of Sebuku Island.

Fo = Mg/(Mg + Fe^{2+}), Whereas Fe^{2+} is as Total iron, n.d.—Not Detected.												
Sample	**SiO$_2$**	**TiO$_2$**	**Al$_2$O$_3$**	**FeO**	**MnO**	**MgO**	**CaO**	**Na$_2$O**	**K$_2$O**	**Cr$_2$O$_3$**	**NiO**	**Total**	**Fo%**
IGN55-1	41.94	0.01	n.d.	4.17	0.07	52.80	0.02	0.01	n.d.	0.92	0.50	100.44	95.76
IGN55-2	42.28	0.01	n.d.	5.98	0.09	51.58	0.03	n.d.	n.d.	0.41	0.45	100.84	93.90
IGN55a-2	42.12	n.d.	n.d.	5.21	0.09	51.77	0.03	n.d.	n.d.	0.40	0.40	100.03	94.66
IGN55a-3	42.60	0.05	n.d.	5.13	0.13	51.61	0.01	n.d.	0.02	0.69	0.45	100.71	94.72
IGN55a-4	42.19	n.d.	n.d.	5.27	0.11	51.10	0.01	0.02	n.d.	0.70	0.39	99.83	94.53
IGN55a-5	41.92	0.01	n.d.	5.47	0.03	52.20	0.02	n.d.	0.01	0.59	0.44	100.71	94.45
IGN55a-6	41.69	n.d.	0.01	5.27	0.11	51.23	0.04	n.d.	n.d.	0.58	0.37	99.30	94.54
IGN55a-7	41.99	0.01	n.d.	5.02	0.11	52.15	0.03	n.d.	n.d.	0.68	0.45	100.48	94.88
IGN55c1-1	41.93	0.01	n.d.	5.84	0.12	52.30	0.02	n.d.	n.d.	0.81	0.44	101.49	94.10
IGN55c1-2	41.94	n.d.	0.02	5.63	0.11	52.36	0.03	n.d.	n.d.	0.53	0.41	101.06	94.31
IGN55c1-3	41.97	n.d.	0.02	5.17	0.13	52.36	0.02	n.d.	n.d.	0.76	0.46	100.90	94.75
IGN55c1-4	41.77	n.d.	n.d.	5.37	0.10	52.27	0.05	0.01	0.01	0.42	0.50	100.51	94.55
IGN85c3-1	41.44	n.d.	0.03	4.57	0.10	53.13	n.d.	n.d.	0.01	0.79	0.43	100.52	95.40

MnO and CaO fall in the overlapping field of olivine from the ophiolite and Alaskan-type chromitites, but they display a very limited variation in their amounts (Figure 8B,C).

The values of Ca versus forsterite in the analyzed olivine are very similar to those of the mantle-hosted olivine proposed by Li et al. [52], having CaO below 0.1 wt% and high forsterite contents (Figure 8C).
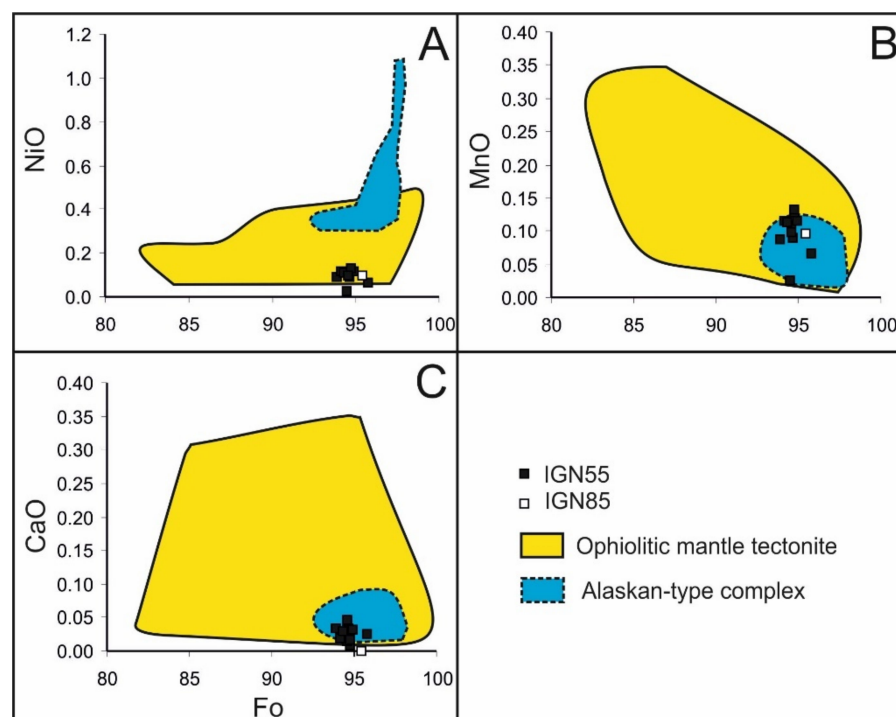
Figure 8. Variation of NiO (**A**), MnO (**B**) and CaO (**C**) as functions of forsterite (Fo) molar % in olivine included in chromite from high-Cr chromitite of Sebuku Island and comparison with olivine associated with chromitite hosted in ophiolitic mantle tectonite and Alaskan-type complex (field from Garuti et al. [45]).

5.2. PGM in the High-Cr Chromitite

The PGM assemblage of the high-Cr chromitite consists of polygonal grains of laurite (<10 μm) included in chromite crystals, sometimes in contact with minute specks of a silicate (Figure 9A,B).
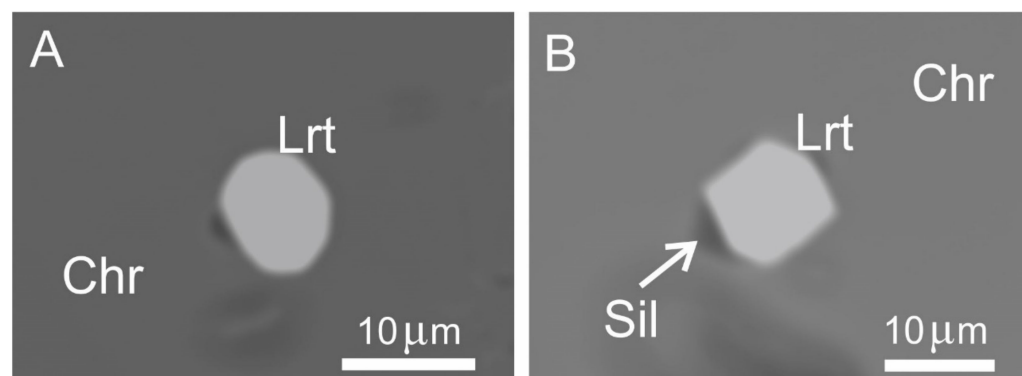

Figure 9. BSE images of polygonal laurite enclosed in chromite of the high-Cr chromitites of Sebuku Island. Single phase crystals (**A**), and in contact with silicate, possible pyroxene (**B**). Abbreviations: Chr—chromite, Lrt—laurite, Sil—silicate.

The compositions of laurite from Sebuku high-Cr chromitite (Table 5) are plotted in the Ru-Os-Ir ternary diagram and compared with those from the Meratus–Bobaris chromitite [31] and from the placers of Pontyn and Tambanio [33,34] (Figure 10). The analyzed laurite is distinguished by its narrow range of Os-Ru substitution corresponding to the Os-Ru atomic ratio in C1 chondrite of 0.74 [53]. The Ru/(Ru + Os) at% ratio in the Sebuku high-Cr chromitite varies from 0.72 to 0.79.

Table 5. Electron microprobe analyses (wt and at%) of laurite from High-Cr and High-Al Chromitite of Sebuku Island.

| Sample	As	S	Ru	Os	Ir	Rh	Pd	Total
n.d.—Not Detetcted.								
High-Crchromitite								
IGN55c2an1	n.d.	31.69	34.70	25.73	2.98	0.70	0.18	95.96
IGN55c2c1an2	n.d.	32.66	36.21	26.55	3.24	0.70	n.d.	99.36
IGN55c2c5an1	0.15	31.98	34.33	22.26	5.16	0.68	0.77	95.34
IGN55c2c5an2	n.d.	32.84	37.82	23.65	5.35	0.70	0.38	100.74
IGN851c3an1	0.39	33.91	36.81	19.26	8.81	0.77	0.63	100.58
IGN851c3an2	0.37	34.54	36.54	19.27	8.99	0.69	0.59	100.98
IGN851c4an1	0.46	34.24	38.69	22.00	2.49	0.81	0.44	99.12
IGN851c4an2	0.45	34.30	38.50	22.00	2.40	0.84	0.58	99.07
IGN851c4an3	0.55	35.51	39.44	22.21	2.46	0.81	0.00	100.98
High-Al chromitite								
IGN338ac3an1	0.44	34.75	37.37	17.12	8.42	0.83	n.d.	98.92
IGN338ac3an2	0.36	34.42	37.62	17.31	8.63	0.94	0.09	99.37
IGN338ac3an3	0.42	34.04	37.72	16.88	8.84	0.89	n.d.	98.79
IGN338ac5an1	0.46	33.72	33.24	17.30	14.17	0.66	n.d.	99.54
IGN338ac5an2	0.37	33.53	32.82	17.03	14.19	0.65	0.03	98.62
IGN338ac7an1	0.35	31.76	28.60	33.16	5.20	0.54	n.d.	99.60
IGN338ac7an2	0.30	31.93	28.69	33.35	4.90	0.59	n.d.	99.77
IGN338ac8an1	0.35	34.80	36.43	20.82	6.61	0.82	n.d.	99.82
IGN338ac8an2	0.30	35.11	36.45	20.70	6.88	0.78	n.d.	100.22
IGN338ac9an1	0.51	32.08	34.08	16.03	16.12	0.87	n.d.	99.68
IGN338bc9an1	0.36	33.60	35.92	18.06	7.73	0.75	0.15	96.57
IGN338bc9an2	0.34	33.71	37.95	18.79	8.51	0.73	0.14	100.16
IGN338bc2an1	0.44	34.69	36.06	19.71	6.94	0.77	n.d.	98.61
IGN338bc2an2	0.44	35.51	36.87	20.12	7.14	0.85	n.d.	100.92
IGN338bc4an1	0.28	34.62	36.90	20.15	7.13	0.74	n.d.	99.82
IGN338bc4an2	0.48	34.52	36.95	20.44	7.34	0.73	n.d.	100.45
IGN338bc5an1	0.34	32.69	27.06	35.37	4.77	0.52	n.d.	100.75
IGN338bc5an2	0.27	32.54	26.79	35.17	4.38	0.59	n.d.	99.74
IGN338bc6an1	0.09	28.86	37.53	22.57	8.20	0.90	n.d.	98.15
IGN338bc7an1	0.52	33.68	36.84	19.93	5.52	0.85	n.d.	97.34
IGN338bc7an2	0.48	34.07	36.78	19.97	5.67	0.87	n.d.	97.84
IGN338bc8an1	0.48	34.90	39.63	18.32	5.06	0.86	n.d.	99.25
IGN338bc9an1	0.56	36.45	43.71	11.05	6.48	0.94	n.d.	99.18
IGN338bc9an2	0.54	36.31	43.50	11.31	6.20	0.88	n.d.	98.73
IGN338bc9an3	0.60	35.25	44.05	11.33	6.56	0.90	n.d.	98.68
IGN338bc10an1	0.46	34.69	37.04	21.10	6.53	0.79	n.d.	100.61
IGN338bc10an2	0.39	34.03	36.79	20.88	6.88	0.72	n.d.	99.67
High-Cr chromitite								
IGN55c2an1	n.d.	66.29	23.03	9.07	1.04	0.45	0.11	100
IGN55c2c1an2	n.d.	66.14	23.26	9.06	1.10	0.44	n.d.	100
IGN55c2c5an1	0.14	66.63	22.69	7.82	1.79	0.44	0.49	100
IGN55c2c5an2	n.d.	65.62	23.97	7.96	1.78	0.44	0.23	100
IGN851c3an1	0.32	66.62	22.94	6.38	2.89	0.47	0.37	100
IGN851c3an2	0.31	67.16	22.54	6.32	2.92	0.42	0.34	100
IGN851c4an1	0.38	66.85	23.97	7.24	0.81	0.49	0.26	100
IGN851c4an2	0.38	66.92	23.83	7.24	0.78	0.51	0.34	100
IGN851c4an3	0.45	67.43	23.75	7.11	0.78	0.48	n.d.	100
High-Al chromitite								
IGN338ac3an1	0.36	67.68	23.09	5.62	2.74	0.51	n.d.	100
IGN338ac3an2	0.30	67.24	23.32	5.70	2.81	0.57	0.05	100
IGN338ac3an3	0.35	67.03	23.56	5.60	2.91	0.55	n.d.	100
IGN338ac5an1	0.39	67.52	21.11	5.84	4.73	0.41	n.d.	100
IGN338ac5an2	0.32	67.67	21.01	5.79	4.78	0.41	0.02	100
IGN338ac7an1	0.31	66.72	19.06	11.74	1.82	0.35	n.d.	100
IGN338ac7an2	0.27	66.82	19.05	11.77	1.71	0.39	n.d.	100
IGN338ac8an1	0.29	67.74	22.50	6.83	2.15	0.50	n.d.	100
IGN338ac8an2	0.25	67.93	22.38	6.75	2.22	0.47	n.d.	100
IGN338ac9an1	0.44	65.78	22.17	5.54	5.51	0.55	n.d.	100
IGN338bc9an1	0.31	67.52	22.90	6.12	2.59	0.47	0.09	100
IGN338bc9an2	0.28	66.42	23.72	6.24	2.80	0.45	0.08	100
IGN338bc2an1	0.37	67.97	22.41	6.51	2.27	0.47	n.d.	100
IGN338bc2an2	0.36	67.97	22.39	6.49	2.28	0.50	n.d.	100
IGN338bc4an1	0.24	67.53	22.83	6.62	2.32	0.45	n.d.	100
IGN338bc4an2	0.40	67.24	22.83	6.71	2.38	0.44	n.d.	100
IGN338bc5an1	0.30	67.63	17.76	12.33	1.65	0.34	n.d.	100
IGN338bc5an2	0.24	67.79	17.71	12.35	1.52	0.39	n.d.	100
IGN338bc6an1	0.08	62.39	25.74	8.23	2.96	0.61	n.d.	100
IGN338bc7an1	0.44	67.18	23.31	6.70	1.84	0.53	n.d.	100
IGN338bc7an2	0.41	67.43	23.10	6.66	1.87	0.54	n.d.	100
IGN338bc8an1	0.40	67.28	24.23	5.95	1.63	0.52	n.d.	100
IGN338bc9an1	0.45	67.76	25.78	3.46	2.01	0.54	n.d.	100
IGN338bc9an2	0.43	67.80	25.77	3.56	1.93	0.51	n.d.	100
IGN338bc9an3	0.49	66.81	26.48	3.62	2.07	0.53	n.d.	100
IGN338bc10an1	0.38	67.32	22.80	6.90	2.11	0.48	n.d.	100
IGN338bc10an2	0.32	67.04	23.00	6.93	2.26	0.44	n.d.	100
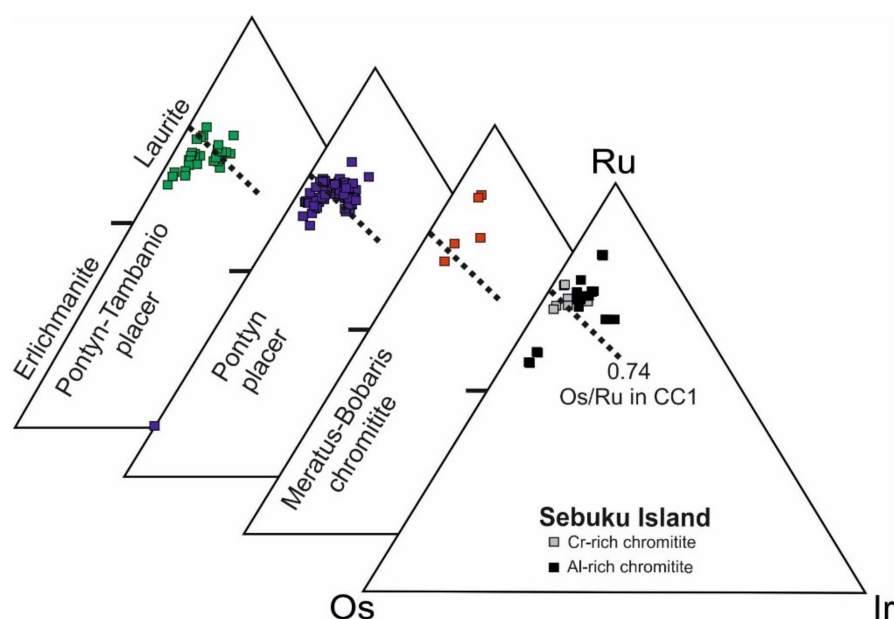
Figure 10. Ru-Os-Ir ternary diagram of the compositions (atomic %) of laurite from Sebuku Island chromitite compared with those from the Meratus–Bobaris chromitite [31] and from the placers of Pontyn and Pontyn–Tambanio [33,34]. Os/Ru ratio (atomic %) calculated from the C1 chondrite [53].

5.3. PGM in the High-Al Chromitite

The PGM associated with the high-Al chromitite of Sebuku Island display a complex mineralogical assemblage consisting of phases of Os, Ir, Ru, Rh and Pt forming single or polyphase grains, varying in size from 1 μm up to about 200 μm. The morphology and the mode of occurrence indicate the presence of both primary and secondary PGM.

Laurite is the only primary PGM occurring as tiny polygonal grains (<20 μm) enclosed in fresh chromite, occasionally in contact with chlorite (Figure 11A,B). Compositions show a wider range of Ru-Os substitution compared with primary laurite from the high-Cr chromitite (Table 5) and, in particular, some grains display marked enrichment in Os with respect to the Os-Ru chondritic ratio of 0.74 (Figure 10). The Ru/(Ru + Os) at% ratio in the high-Al chromitite of Sebuku Island is comprised between 0.59 and 0.88. One euhedral grain of laurite surrounded by chlorite (Figure 12A) is associated with cuproiridsite (ideal $CuIr_2S_4$) and contains lamellae of Ir oriented along crystallographic planes.
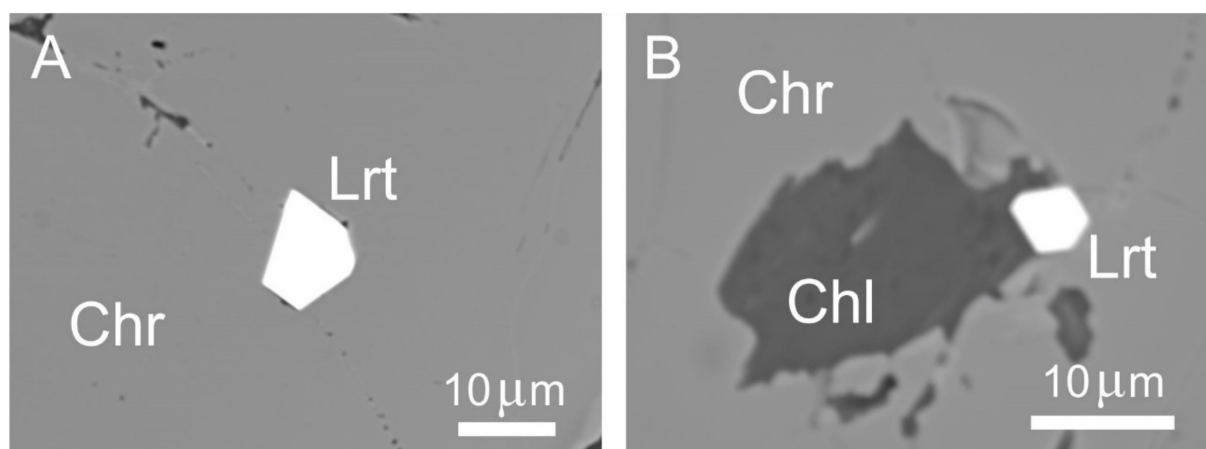

Figure 11. BSE images of polygonal laurite associated with the high-Al chromitites of Sebuku Island showing a single grain enclosed in chromite crystals (**A**), and in contact with chlorite (**B**). Abbreviations: Chr—chromite, Lrt—laurite, Chl—chlorite.
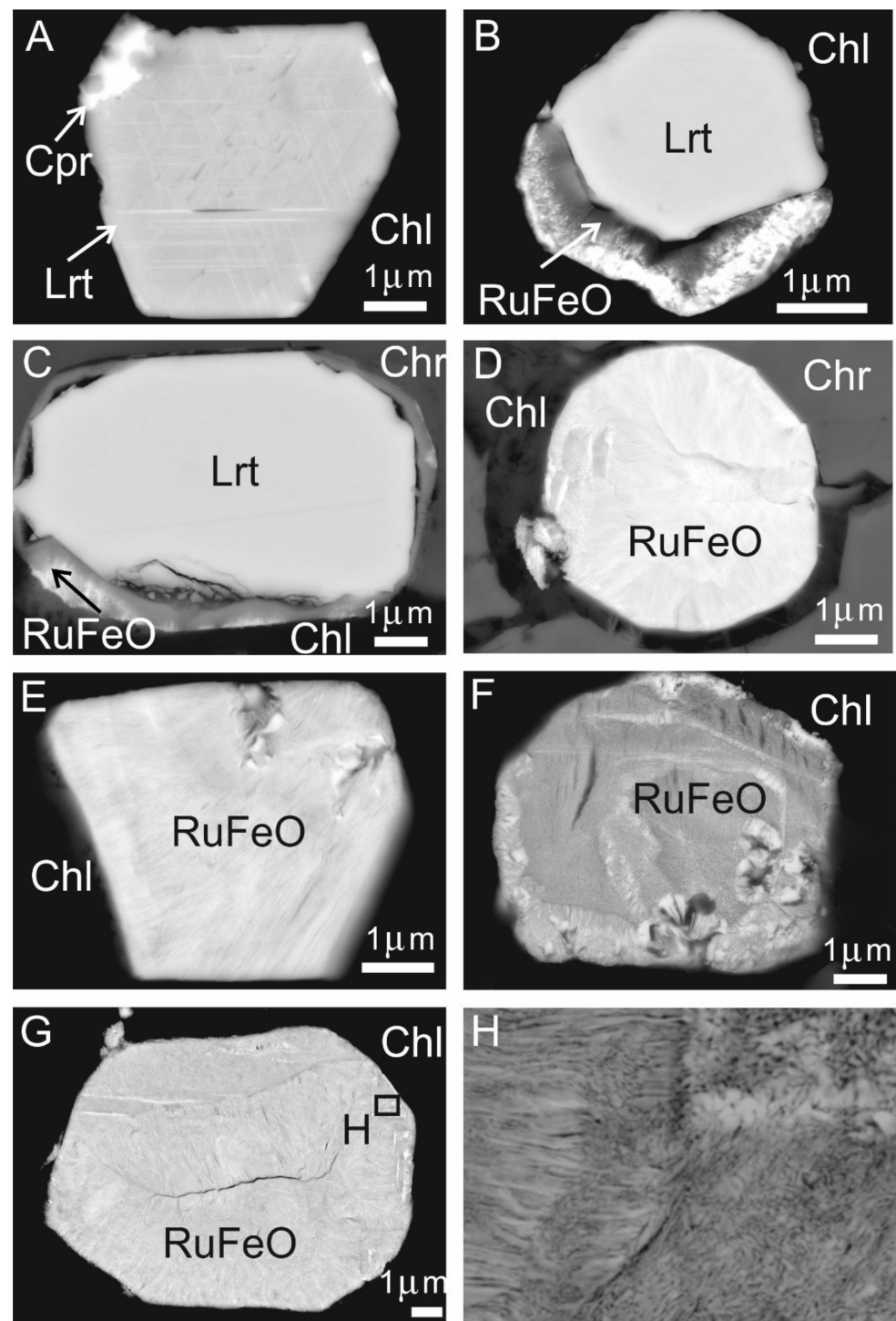
Figure 12. Field emission (FE-SEM) images of PGM associated with the chromitites of Sebuku Island showing euhedral laurite in contact with cuproiridsite and lamellae of iridium (**A**), unaltered core of laurite rimmed by Ru-Os-Ir-Fe-O phase (**B**–**D**), polygonal grains of Ru-Os-Ir-Fe-O occurring in contact with chlorite (**E**–**G**), enlargement of the grain of Figure (**G**,**H**). Abbreviations: Chr—chromite, Lrt—laurite, Chl—chlorite, Cpr—cuproiridsite, RuFeO—compounds of Ru-Os-Ir-Fe-O.

Some composite and pseudomorphic crystals of PGM were found in contact with altered silicates and consist of an unaltered core of laurite rimmed by a heterogeneous compound of Ru-Os-Ir-Fe-O (Figure 12B,C), characterized by low reflectance and a fibrous texture, similar to the compounds previously described from chromitites of several ophiolite complexes [13,20,54–57]. Other grains occurring at the contact chromite–chlorite, or within

chlorite fractures, are characterized by a polygonal to sub-rounded shape (Figure 12E–H) and appear to be composed of the same material that constitutes the laurite rim (Ru-Os-Ir-Fe-O). Electron-microprobe analyses (Table 6) reveal that the Ru-Os-Ir-Fe-O phase has Ru-Os-Ir relationships very similar to that of the laurite core or the primary laurite included in fresh chromite (Figure 13).

Table 6. Electron microprobe analyses (wt%) of PGE-bearing oxygenated compounds from high-Al chromitite of Sebuku Island.

n.d.—Not Detetcted.

| Sample	S	As	O	Os	Ir	Ru	Rh	Pt	Pd	Fe	Ni	Cu	Mn	Total
IGN338d6-1	0.06	0.60	9.00	23.22	9.94	38.71	1.44	n.d.	n.d.	11.38	1.85	n.d.	n.d.	96.20
IGN338d6-2	n.d.	0.48	8.94	24.65	9.27	38.17	1.23	n.d.	0.22	11.35	2.03	n.d.	n.d.	96.34
IGN338d6-3	0.03	0.52	8.48	23.58	10.50	38.39	1.20	n.d.	n.d.	11.87	1.91	n.d.	n.d.	96.47
IGN338ac3-1	0.02	0.51	5.91	36.71	4.90	35.52	1.01	n.d.	0.54	4.25	6.17	n.d.	0.30	95.84
IGN338ac3-2	n.d.	0.45	6.27	36.46	4.75	35.16	0.90	n.d.	0.31	4.37	5.92	n.d.	0.30	94.88
IGN338ac3-3	n.d.	0.71	10.80	25.31	4.33	45.78	1.41	n.d.	n.d.	7.82	2.71	n.d.	0.31	99.18
IGN338ac3-4	0.02	0.45	6.23	36.40	4.66	34.35	1.07	n.d.	n.d.	4.78	5.94	n.d.	0.31	94.21
IGN338ac3-5	n.d.	0.48	5.31	36.86	5.27	36.02	1.01	n.d.	n.d.	4.35	6.12	n.d.	0.33	95.74
IGN338ac3-6	n.d.	0.47	6.41	35.74	4.66	34.87	1.16	n.d.	0.22	5.02	5.81	n.d.	0.35	94.71
IGN338ac3-7	0.04	0.75	9.05	23.69	4.41	48.50	1.44	n.d.	n.d.	7.53	0.87	n.d.	0.41	96.67
IGN338ac3-8	0.08	0.70	8.43	24.26	5.13	49.12	1.49	n.d.	n.d.	7.76	0.97	n.d.	0.47	98.39
IGN338c4-1	0.02	0.38	7.84	23.69	8.42	44.86	1.38	n.d.	n.d.	4.59	0.73	n.d.	0.49	92.40
IGN338c4-2	0.01	0.39	11.71	23.77	9.65	35.88	1.04	n.d.	n.d.	12.74	1.77	n.d.	0.55	97.52
IGN338bc1-1	n.d.	0.77	13.29	15.16	11.00	40.74	1.75	n.d.	0.71	1.73	2.03	0.11	12.91	100.20
IGN338bc1-2	0.02	0.69	13.07	15.29	11.09	41.22	1.57	n.d.	0.66	1.68	2.12	0.15	12.96	100.51
IGN338bc1-3	0.02	0.76	13.47	15.16	10.43	41.52	1.42	n.d.	0.33	1.65	1.91	0.11	12.98	99.76
IGN338bc1-4	0.03	0.67	12.85	15.03	10.94	40.76	1.32	n.d.	0.63	1.66	2.01	0.15	13.21	99.26
IGN338bc1-5	0.01	0.66	13.41	15.03	10.75	41.15	1.44	n.d.	0.40	1.65	2.03	0.14	13.54	100.20
IGN338bc1-6	n.d.	0.65	19.05	13.75	9.69	33.48	1.24	n.d.	0.80	2.15	2.19	n.d.	17.56	100.57
IGN338bc1-7	0.01	0.52	20.28	13.16	9.50	32.60	1.13	n.d.	0.17	2.20	2.08	n.d.	18.06	99.72
IGN338bc1-8	0.01	0.51	20.12	13.79	9.85	32.02	1.18	n.d.	0.68	2.22	2.18	n.d.	18.15	100.70
IGN338bc1-9	n.d.	0.54	19.98	13.13	9.81	32.04	1.16	n.d.	0.96	2.13	2.19	n.d.	18.35	100.30
IGN338bc1-10	n.d.	0.54	20.35	12.86	9.73	30.74	1.16	n.d.	0.34	2.20	2.34	n.d.	19.09	99.36
IGN338dc2-1	0.03	0.00	39.20	0.09	0.16	n.d.	n.d.	0.24	n.d.	0.25	7.86	n.d.	39.83	87.65
IGN338dc2-2	0.01	0.00	39.41	0.02	0.01	0.02	n.d.	0.50	n.d.	0.90	5.89	n.d.	43.18	89.93
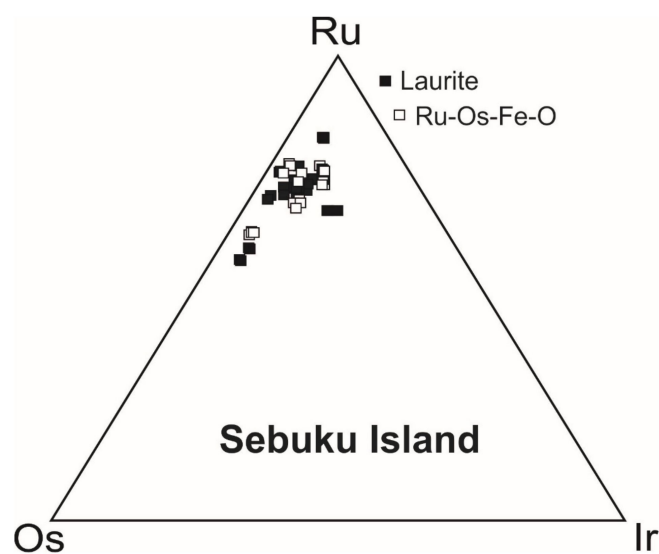
Figure 13. Ru-Os-Ir ternary diagram of the compositions (atomic %) of laurite and Ru-Os-Ir-Fe oxygenated compounds from Sebuku chromitite.

Other phases carrying PGE in the high-Al chromitites are characterized by an irregular shape and a consistent association with chlorite in the interstitial silicate matrix or along cracks. The BSE images and the elemental distribution maps show the complexity of the internal texture of these PGM and emphasize the consistent presence of As, Fe, Ni, Cu and Mn (Figures 14–20).
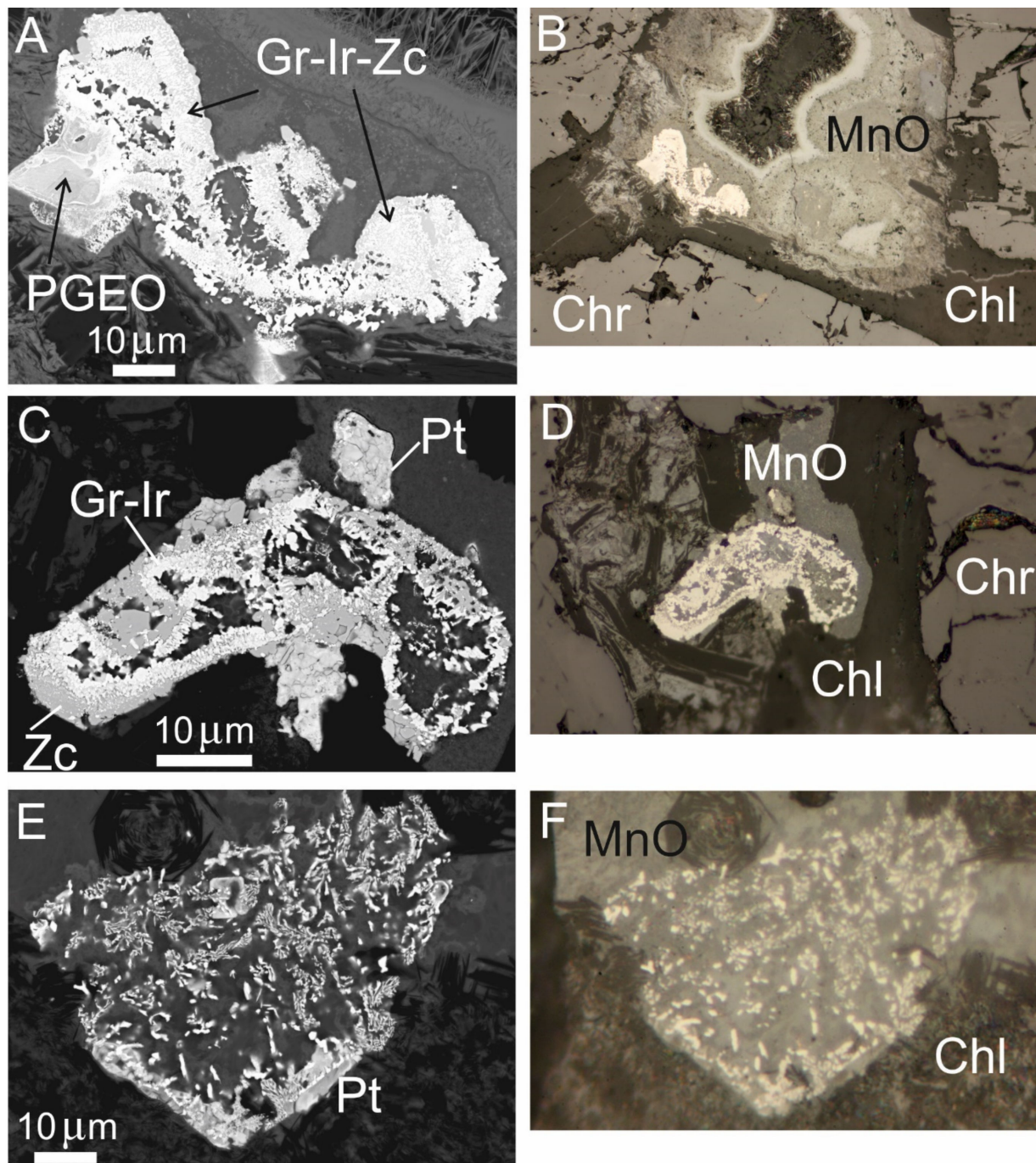

Figure 14. FE-SEM images (**left row**) and reflected-light optical microscopic images (**right row**) showing secondary PGM that occur associated with the interstitial chlorite and Mn-Cr-Fe-Ni hydroxides from the high-Al chromitite of Sebuku Island. Grains with an irregular and complex shape (**A–D**) and sponge-textured PGM grain composed of iridium rimmed by an alloy of Pt-Fe-Cu (**E,F**). Abbreviations: Chr—chromite, Chl—chlorite, Ir—iridium, Gr—garutiite, Zc—zaccariniite, PGEO—compound of Ru-Mn-Os-Ir-Fe-O, Pt—platinum alloy.
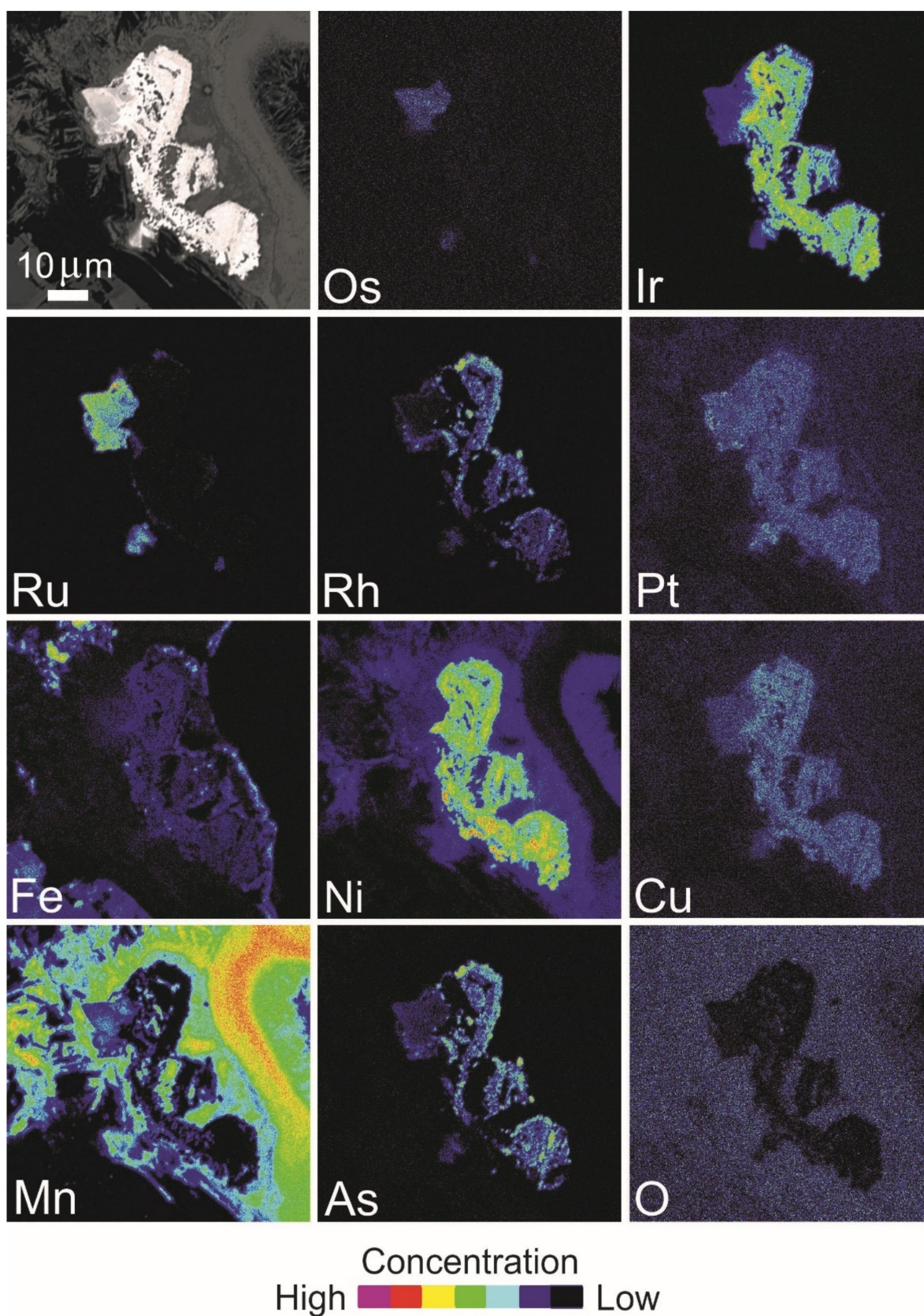
Figure 15. BSE image and X-ray elemental distribution maps of Os, Ir, Ru, Rh, Pt, Fe, Ni, Cu, Mn, As and O in the PGM shown in Figure 14A,B composed of garutiite–iridium–zaccariniite and a compound of Ru-Mn-Os-Ir-Fe-O.
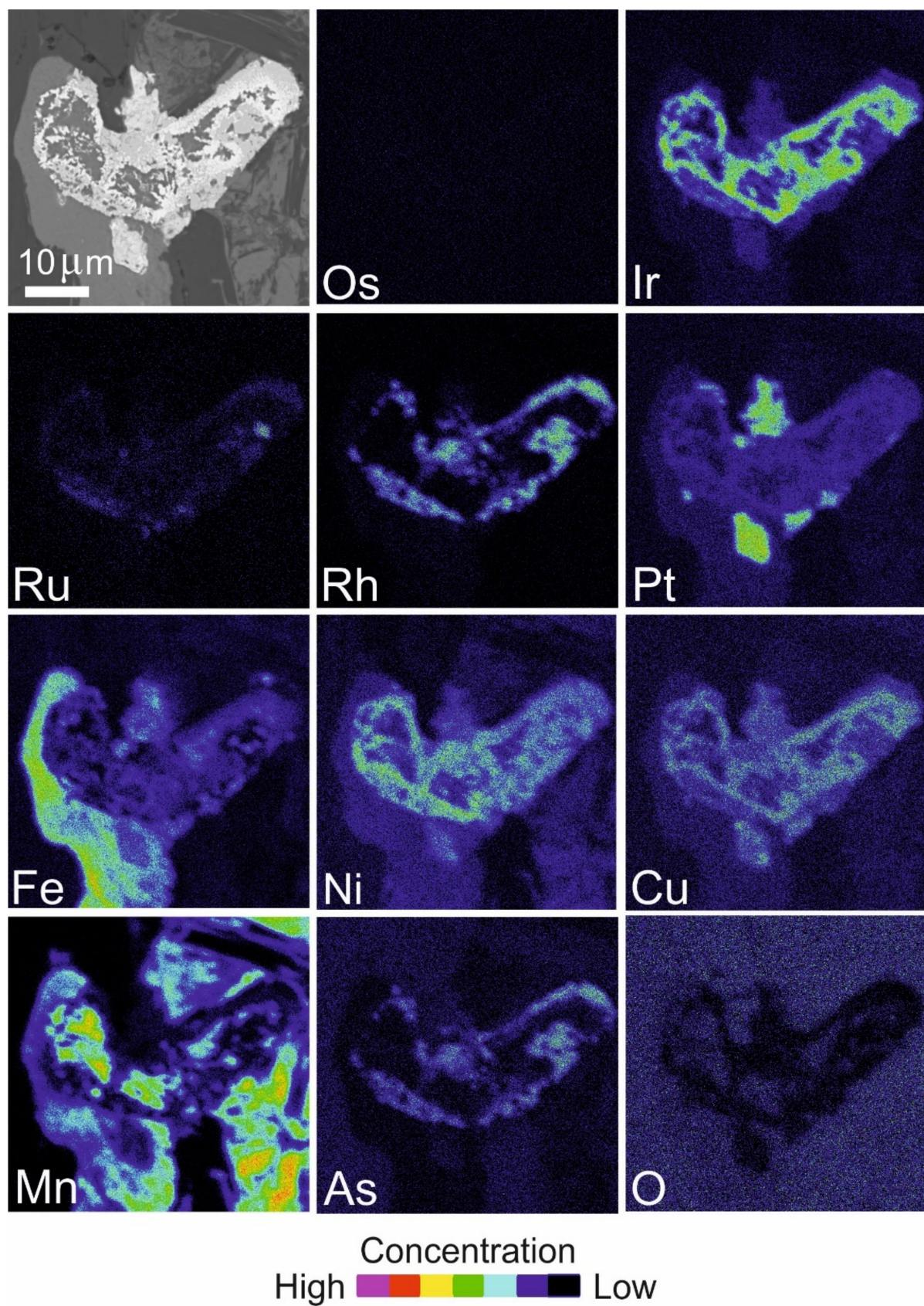
Figure 16. BSE image and X-ray elemental distribution maps of Os, Ir, Ru, Rh, Pt, Fe, Ni, Cu, Mn, As and O in the PGM shown in Figure 14C,D composed of garutiite–iridium–zaccariniite and a Pt alloy.
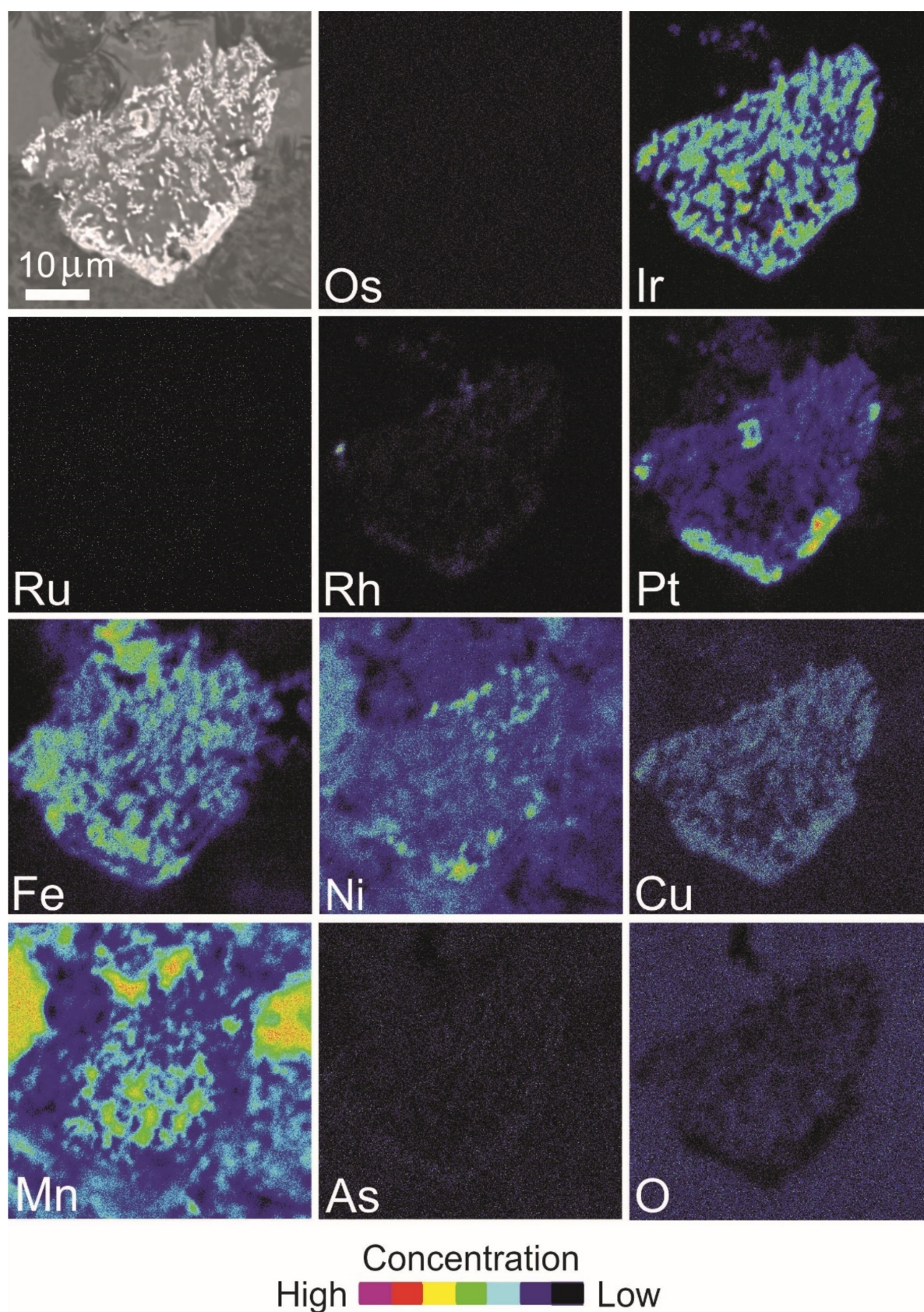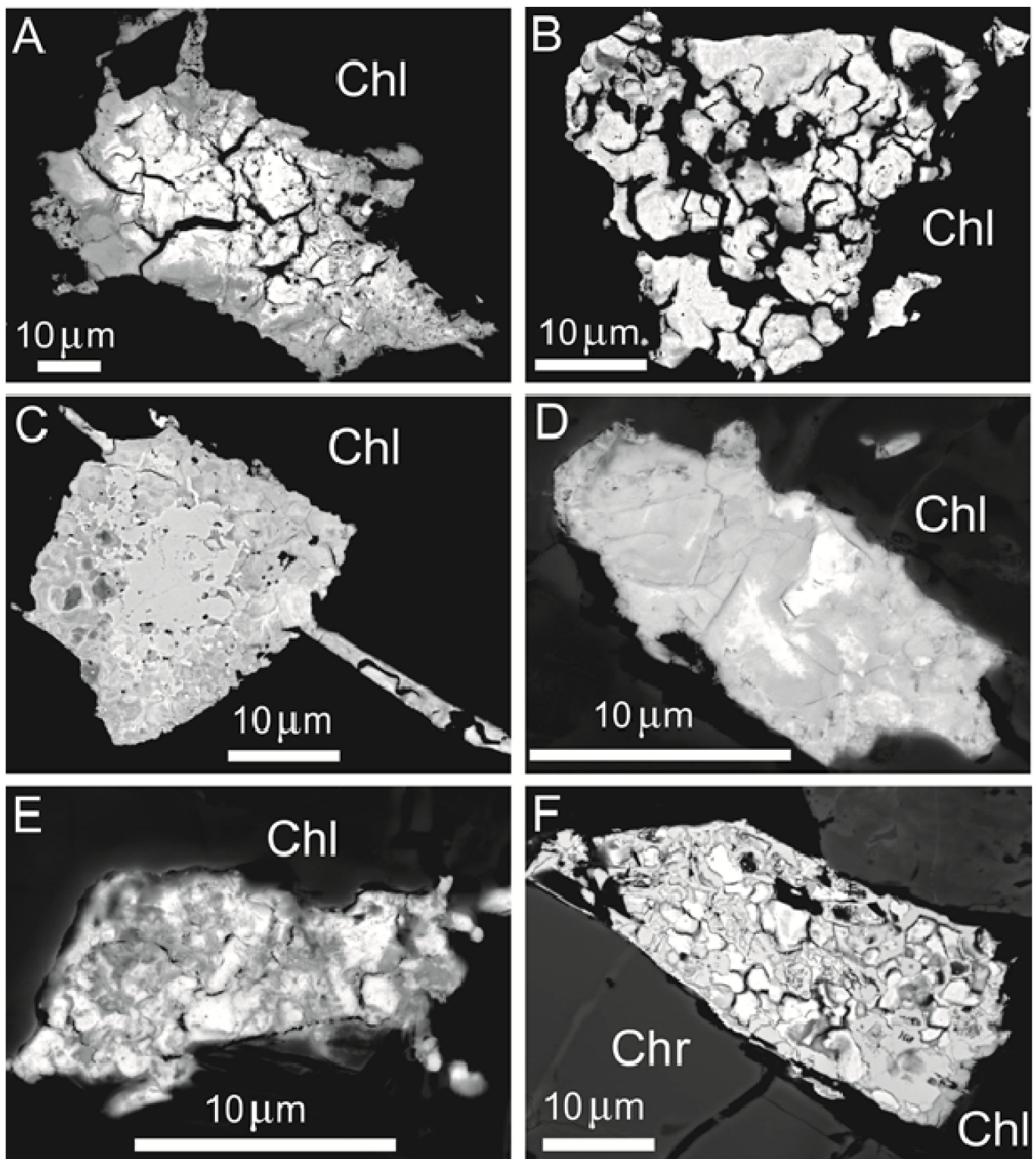
Figure 17. BSE image and X-ray elemental distribution maps of Os, Ir, Ru, Rh, Pt, Fe, Ni, Cu, Mn, As and O in the PGM shown in Figure 14E,F, composed of iridium and a Pt alloy.

Figure 18. FE-SEM images of Pt-bearing alloys found in high-Al chromitite of Sebuku Island revealing a porous texture, irregular shape and zoning, enclosed in chlorite (**A**–**E**) and in the contact of chromite and chlorite (**F**). Abbreviations: Chr—chromite, Chl—chlorite.
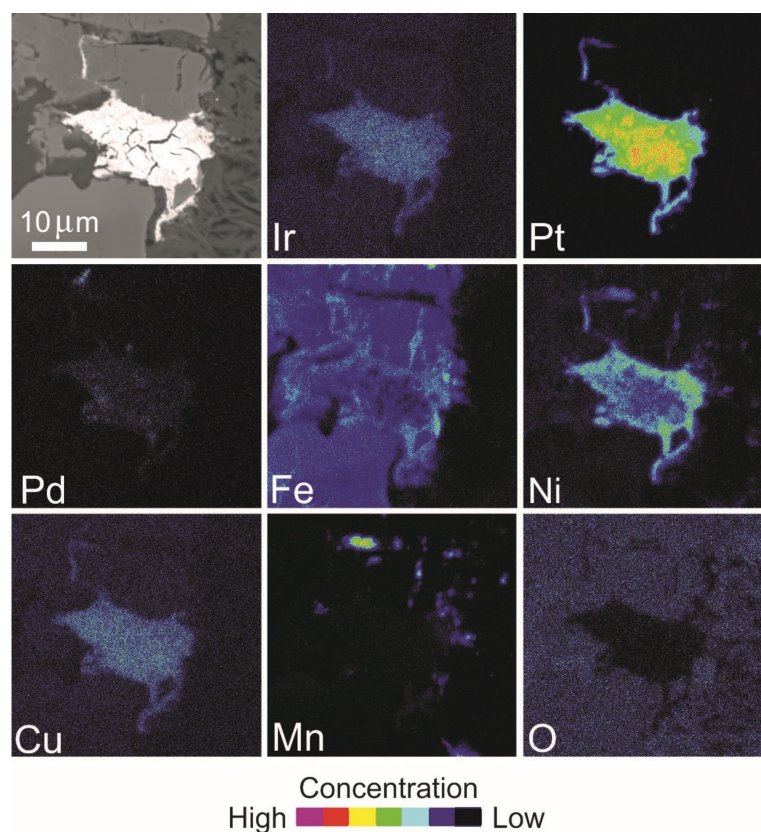
Figure 19. BSE image and X-ray elemental distribution maps of Ir, Pt, Pd, Fe, Ni, Cu, Mn and O in the Pt alloy of Figure 18A.
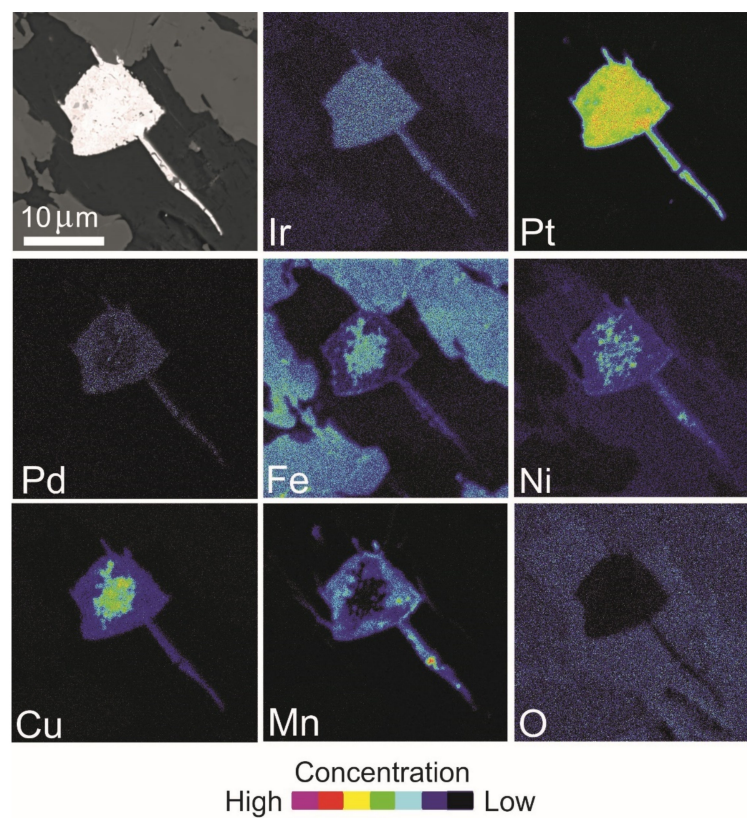
Figure 20. BSE image and X-ray elemental distribution maps of Ir, Pt, Pd, Fe, Ni, Cu, Mn and O in the Pt alloy of Figure 18C.

Some large grains (~200 μm) are typically associated with Mn-Cr-Fe-Ni hydroxides (Figure 14A–F). Two grains contain the association of iridium, zaccariniite (ideal RhNiAs) and garutiite (ideal Ni,Fe,Ir) (Table 7, Figure 14A,C). Small particles of Pt-Fe alloy are associated with grains in Figure 14C,E. Of particular interest is the presence of an unusual PGM composed of Ru-Mn-Os-Ir-Fe-O (Table 6, Figure 14A) that may correspond to the phase described from chromitites of the Pirogues ophiolite in New Caledonia [11]. One grain composed of iridium rimmed by an alloy of Pt-Fe-Cu occurs in contact with Mn-hydroxide and shows a sponge texture (Figure 14E,F) similar to the so-called "weathered and disordered" PGM described by Bowles and Suárez [58].

Table 7. Electron microprobe analyses (wt and at %) of Pt-bearing alloys and garutiite from High-Al Chromitite of Sebuku Island.

| n.d.—Not Detetcted. | | | | | | | | | | | | | |
Sample	S	As	Os	Ir	Ru	Rh	Pt	Pd	Fe	Ni	Cu	Mn	Total
Pt-bearing alloys													
IGN338dc2	0.11	0.09	0.16	n.d.	0.06	0.23	71.55	1.35	16.88	9.50	n.d.	0.53	100.46
IGN338dc4-1	0.47	n.d.	0.12	n.d.	n.d.	0.28	81.15	2.77	11.20	4.17	n.d.	1.09	101.25
IGN338dc4-2	0.53	n.d.	0.14	n.d.	n.d.	0.11	84.73	1.56	8.15	3.40	n.d.	1.00	99.63
IGN338dc4-3	0.37	0.01	0.11	n.d.	n.d.	0.27	85.24	2.09	6.72	3.98	n.d.	0.78	99.58
IGN338dc4-4	0.49	n.d.	0.22	n.d.	n.d.	0.16	85.31	2.20	6.82	3.73	n.d.	0.86	99.79
IGN338dc4-1	0.37	n.d.	n.d.	n.d.	n.d.	0.13	85.38	2.67	6.95	4.11	n.d.	0.76	100.37
IGN338dc3-1	0.11	n.d.	n.d.	n.d.	0.01	0.21	85.69	4.34	5.63	3.20	n.d.	1.24	100.42
IGN338dc1-1	0.15	n.d.	0.01	n.d.	0.10	0.33	89.91	1.93	5.10	2.24	n.d.	0.19	99.96
IGN338dc1-1	0.13	n.d.	0.14	n.d.	0.10	0.28	91.68	2.01	3.71	2.02	n.d.	0.21	100.28
Garutite													
IGN338bc1-1	0.02	0.43	0.60	55.04	1.81	0.50	n.d.	1.06	3.46	36.05	1.22	0.48	100.68
IGN338bc1-2	n.d.	0.12	0.19	56.15	1.09	n.d.	n.d.	0.07	3.58	36.13	1.19	1.70	100.21
Pt-bearing alloys													
IGN338dc2	0.39	0.13	0.10	n.d.	0.07	0.26	42.58	1.48	35.08	18.79	n.d.	1.13	100
IGN338dc4-1	1.95	n.d.	0.08	n.d.	n.d.	0.36	55.36	3.47	26.70	9.45	n.d.	2.63	100
IGN338dc4-2	2.40	n.d.	0.10	n.d.	n.d.	0.16	62.98	2.13	21.16	8.41	n.d.	2.65	100
IGN338dc4-3	1.72	0.02	0.09	n.d.	n.d.	0.38	64.83	2.91	17.86	10.07	n.d.	2.12	100
IGN338dc4-4	2.25	n.d.	0.17	n.d.	n.d.	0.23	64.57	3.05	18.02	9.38	n.d.	2.32	100
IGN338dc4-1	1.71	n.d.	n.d.	n.d.	n.d.	0.19	63.99	3.67	18.20	10.24	n.d.	2.02	100
IGN338dc3-1	0.49	n.d.	n.d.	n.d.	0.02	0.30	66.23	6.15	15.19	8.22	n.d.	3.40	100
IGN338dc1-1	0.75	n.d.	0.01	n.d.	0.16	0.51	74.25	2.92	14.71	6.14	n.d.	0.55	100
IGN338dc1-1	0.69	n.d.	0.12	n.d.	0.16	0.46	78.05	3.14	11.04	5.73	n.d.	0.63	100
Garutite													
IGN338bc1-1	0.07	0.55	0.30	27.72	1.74	0.47	n.d.	0.97	6.00	59.47	1.86	0.84	100
IGN338bc1-2	n.d.	0.16	0.10	28.22	1.04	n.d.	n.d.	0.06	6.18	59.46	1.80	2.99	100

Several Pt-bearing alloys have been found exclusively in the matrix or along cracks of the host chromitite (Table 7, Figure 18A–F), but never enclosed in fresh chromite crystals. The alloys display a porous texture and irregular shape and are chemically inhomogeneous. Elemental distribution maps (Figures 19 and 20) are reported for two selected grains shown in Figure 18A,C, indicating Pt as the major PGE accompanied by minor Ir and very low traces of Pd, in one case. The base metals Fe, Cu and Ni are alternatively enriched at the core or at the rim of the grains, whereas Mn is visible in the rim of grain in Figure 18C. Trace amounts of Pd have been detected and O is absent. The map of Figure 20 shows that Ir and Cu are homogenously distributed. The core of the grain is enriched in Pt and the rim is enriched in Fe and Ni. Palladium, Mn and O are absent. The compositions (at%) of the Pt-bearing alloys from Sebuku high-Al chromitite are plotted in the ternary diagram of Figure 21 and compared with those from the placers of Riam Kanan and Pontyn [34]. The analyzed alloys in the high-Al chromitite of Sebuku are enriched in Ni, Fe and Cu.
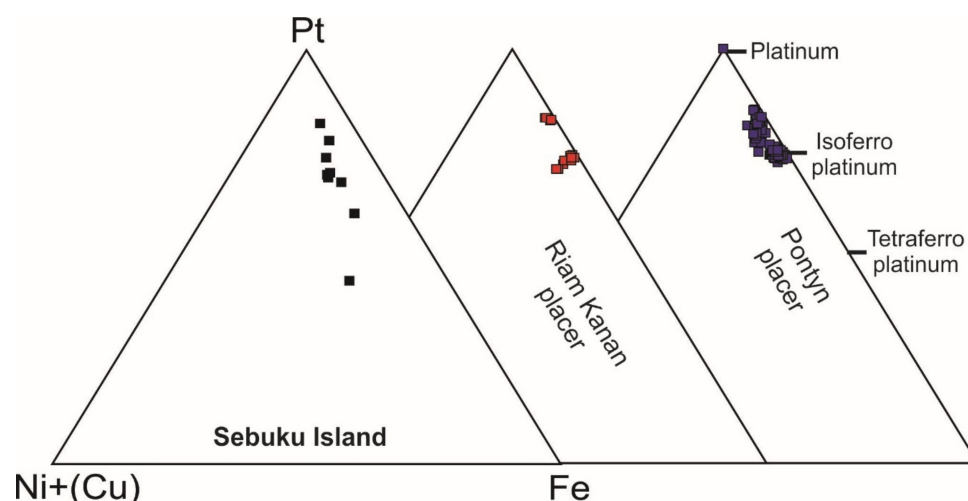
Figure 21. Pt-Fe-Ni + (Cu) ternary diagram of the compositions (atomic %) of the Pt-bearing alloys from the Sebuku high-Al chromitites and compared with those from the placers of Riam Kanan and Pontyn [34].

6. Discussion

6.1. The Significance of the Chromite Composition and Associated Silicates

The precipitation of the ophiolitic chromitites is mainly controlled by the following factors: (1) the degree of partial melting of the mantle source, (2) the composition of the parent magma, (3) the reactions between the residual mantle and the percolating magma, (4) the presence of metasomatic fluids and (5) the geodynamic environment in which the chromitites formed [18,41,44–47,59–76]. The composition of the chromite is related to the nature of the melts, and several authors have suggested that high-Cr chromitites represent the results of metasomatic reactions between the residual mantle and the percolating hydrous high-Mg boninitic melts, typical of the SSZ [44–47,62,63,66,67,70,74]. The high-Al chromitite formed by the reaction of a mantle peridotite with an aluminous melt in the MOR environment [60,61,65–67] or in the back arc basin (BAB) of the ophiolite [70,77–79]. Alternatively, a model in which the high-Al chromitite formed during the early stage of proto-forearc in an SSZ setting subduction was proposed by several authors [80,81]. The coexistence of high-Al and high-Cr chromitites within the same ophiolite complex has been interpreted to have been formed in two different geodynamic settings, during the regression of the oceanic lithosphere from the MOR towards SSZ. [62,63,67]. Alternatively, a bimodal distribution and vertical zoning with the high-Cr type being located in the deep mantle section and the high-Al type occurring higher in the stratigraphy, close to the Moho transition during differentiation of a single melt with initial high-Cr boninitic composition in an SSZ, has been proposed [8,9,46,47,67,73,74].

The data presented in this contribution, suggest that the chromitites from Sebuku Island formed through the later model, although the initial composition of the melt has a tholeiitic affinity rather than boninitic. This assumption is supported by the chromite composition. According to the graphics of Figure 6A,B, all the high-Cr chromitites are consistent with an origin in an SSZ. Furthermore, the associated olivine displays a composition compatible with those observed in olivine associated with hosted mantle chromitite (Figure 8A–C), and the presence of abundant serpentine in the altered matrix indicates that the most abundant magmatic silicate was olivine.

6.2. Evolution of the PGM from the Magmatic Stage to Low T Regime

The IPGE are more refractory and less chalcophile than the PPGE. Therefore, the IPGE are more concentrated in chromitite, while PPGE tend to follow the sulfides (Naldrett and von Gruenevaldt, 1989). For these reasons, most of the PGM that occur enclosed in fresh chromite consist of Ru-Os-Ir phases, such as sulfides of the laurite–erlichmanite series and

alloys in the Os-Ir-Ru system. In the magmatic stage, laurite is in equilibrium with Os-Ir-Ru alloys at a T around 1300 °C and relatively low fS_2. Laurite becomes progressively enriched in Os with decreasing T and increasing fS_2, to reach the stability field of erlichmanite [6,7].

Laurite is the only magmatic PGM observed in both the high-Al and the high-Cr chromitites of the Sebuku Island ophiolite. The absence of alloys in the Os-Ir-Ru system and erlichmanite suggest that magmatic laurite in the Sebuku chromitite crystallized in a narrow range of fS_2 and T. However, laurite found in the high-Al chromitite is slightly enriched in Os (Figure 10) compared with those occurring in the high-Cr chromitite.

Therefore, we can argue that it crystallized at higher fS_2 and lower T, consistently with the hypothesis that the host high-Al chromitite crystallized from a more evolved melt.

Besides evolved magmatic laurite, the high-Al chromitite contains a great number of secondary PGM, i.e., altered at low T during post magmatic processes (Figures 12, 14 and 18). Several secondary PGM containing Ru-Os-Ir-Fe-O as a major component have been analyzed. Based on their morphology, texture and composition they consist, very likely, of a mixture of ruthenium and magnetite as previously described in the chromitite of Loma Peguera ophiolite [82].

As previously reported by several authors, we also suggest that the PGM found in the studied chromitite derived by in situ desulfuration of laurite at low T desulfuration with substitution of the removed S by O and Fe [13,53–57]. This process took place apparently without change in volume, since the external shape of the original sulfide crystal is generally preserved (Figure 12B–G).

This hypothesis is supported by the fact that the composition (at%) of the Ru-Os-Ir-Fe-O in terms of Ru-Os-Ir overlaps the field of the coexisting laurite (Figure 13) and by the finding of several grains that consist of a laurite core rimmed by the Ru-Os-Ir-Fe-O (Figure 12B–D). Another example of secondary PGM is reported in Figure 12A. In this case, the iridium lamellae arranged along the crystallographic plans of the host laurite are considered to represent an ex-solution product formed after the magmatic precipitation of laurite. The PGM was originally trapped as a tiny sulfide bleb containing Ru, Os, Ir and Cu at high T. Laurite can accommodate in its lattice only a limited amount of Cu and Ir; therefore, during the post-magmatic cooling the excess of these two elements was consumed to form the tiny Ir lamellae and the cuproiridsite grain located in the external edge of the host laurite (Figure 12A).

All these observations point to an origin in the ophiolitic mantle for the high-Cr overlapping field of SSZ and MOR chromitites (Figure 6B). However, the diagram of Figure 6A shows that they are compatible with the chromitite associated with the supra-Moho cumulates of the Urals and Sulawesi Island SSZ ophiolites [45,46]. The higher content of V_2O_5 detected in the high-Al chromitite compared with those of the high-Cr chromitite (Figure 5E) is also consistent with this model.

Iridium, garutiite and zaccariniite occur exclusively in the secondary PGM assemblage of the high-Al chromitite of Sebuku Island. As previously reported by several authors, these PGM precipitated at low T during the serpentinization and/or laterization of the host ophiolite complex [56,83,84]. Iridium, garutiite and zaccariniite observed in the studied chromitite present a dendritic texture (Figure 14), then can suggest a neo-formation and crystallization of these PGM directly from low T secondary fluids [27,28].

In some cases, they occur in close association with the uncommon PGM composed of Ru, Mn, Os, Ir, Fe and O, chlorite and Mn-Cr-Fe-Ni hydroxides. A similar PGM assemblage was reported in New Caledonia chromitites and derived placer deposits [11,12]. This assemblage resulted from the alteration of magmatic PGM and the precipitation of oxides in lateritic conditions, suggesting the existence of mechanisms of transport and crystallization of PGM in surface conditions [11,12]. The proposed mechanisms contributed to the redistribution, mobilization and enrichment of PGE in laterite [11,12]. Therefore, we can argue that the pseudomorphic Ru-Os-Ir-Fe-O found in the Sebuku chromitites were altered during the serpentinization at T well below 300 °C, as indicated by the chlorite

geothermometer, whereas the neo-formed PGM, such as garutiite, zaccariniite and iridium, precipitate during the laterization process that affected the host ophiolite.

The boninites represent highly sulfur-undersaturated mafic magmas, because they have formed from a strongly depleted mantle source that has lost most, if not all, of its original sulfide phase [59]. This implies that the sulfur saturation rarely is achieved during the precipitation of high-Cr chromitite within an ophiolitic mantle. On the contrary, tholeiitic magma can be S-saturated and the reaction between this melt and depleted harzburgites can be responsible for the precipitation of high-Al chromitite [59].

The presence of abundant PPGE minerals in mantle-hosted ophiolitic chromitites was rarely observed. However, in the few cases described, the model suggested for their crystallization was similar to those proposed by Naldrett and von Gruenevaldt [4], who suggested that both ophiolitic and stratiform chromitites enriched in PPGE had to have contained significant amounts of magmatic Ni-Cu-Fe sulfides at the time of their deposition as the result of the formation of an immiscible sulfide liquid.

The sulfide segregating in the final stages of the chromite event acted as the collector for the most chalcophile Pd, Pt and to a lesser extent Rh, that precipitated in specific PGM, generally confined to the interstitial silicate matrix of the chromitite. This model can be applied to explain the presence of abundant Pt-bearing alloys occurring in the altered matrix of the host high-Al chromitite of Sebuku Island, since they formed from an evolved magma with an initial S-saturated tholeiitic composition and not from a boninitic melt and precipitate close to the Moho as previously proposed by Prichard et al. [9] for the Al'Ays chromitites. The magmatic precursors of the Pt-alloys probably were sulfides that, similarly to the Ru-Os-Ir-Fe-O, were affected by a desulfuration process at low T during serpentinization and lateritization, as suggested also for the formation of the secondary PGM described in the New Caledonia chromitites [11]. This assumption is corroborated by the irregular shape of the Pt-bearing alloy, their porosity and their puzzling zoning that suggest substitution of Ni, Fe, Mn and less Cu for S.

7. Summary and Concluding Remarks

The Sebuku Island ophiolite includes high-Al and high-Cr chromitites that formed in an SSZ due to interaction between the residual mantle and the tholeiitic magma. The resulting melt underwent differentiation precipitating high-Cr chromitite in the deep mantle and the high-Al ones in the upper transition zone, close to the Moho.

The high-Cr chromitite contains laurite included in chromite crystals as the only magmatic IPGE phase. On the basis of their morphology and composition, the laurite from the high-Cr chromitite of Sebuku Island can be classified as a primary PGM, formed at high magmatic T. The high-Al chromitite comprises a more complex PGM assemblage consisting of primary magmatic laurite enriched in Os and a suite of secondary PGM composed of alloys (garutiite, iridium, ruthenium intergrown with magnetite and Pt-Fe-Ni phases), zaccariniite and PGE-bearing Mn oxides.

The presence of abundant irregular-in-shape alloys in the Pt-Fe-Ni system in the altered matrix of the chromitite suggests that the fS_2 in the tholeiitic parent melt high-Al chromitite increased by differentiation and was high enough to collect the PPGE in interstitial sulfides during the magmatic precipitation of chromite.

The strong serpentinization and weathering that affect the Sebuku Island ophiolite caused the alteration of PGM located in the interstitial silicate matrix. The original PGE sulfides underwent desulfuration, forming aggregates of native Ru-Ir-Os intergrown with magnetite at the expenses of laurite, and a variety of Pt-Fe-Ni alloys at the expenses of PPGE sulfides. Garutiite, iridium and zaccariniite crystallized from secondary fluids during the laterization process that affected the host ophiolite.

Chromitite similar to the high-Al found in Sebuku Island potentially can be the lode deposit of the PGE nuggets previously reported in Borneo [32–34].

References

1. Mansur, E.; Ferreira Filho, C. Chromitites from the Luanga Complex, Carajás, Brazil: Stratigraphic distribution and clues to processes leading to post-magmatic alteration. *Ore Geol. Rev.* **2017**, *90*, 110–130. [CrossRef]
2. Thayer, T.P. Chromite segregations as petrogenetic indicators. In *Symposium on the Bushveld Igneous Complex and Other Layered Intrusions*; Geological Society of South Africa: Johannesburg, South Africa, 1970; Volume 1, pp. 380–390.
3. Dick, H.J.B.; Bullen, T. Chromian spinel as a petrogenetic indicator in abyssal and alpine-type peridotites and spatially associated lavas. *Contrib. Mineral. Petrol.* **1984**, *86*, 54–76. [CrossRef]
4. Naldrett, A.J.; Von Gruenevaldt, G. The association of PGE with chromitite in layered intrusions and ophiolite complexes. *Econ. Geol.* **1989**, *84*, 180–187. [CrossRef]
5. Tsoupa, G.; Economou-Eliopoulos, M. High PGE contents and extremely abundant PGE-minerals hosted in chromitites from the Veria ophiolite complex, northern Greece. *Ore Geol. Rev.* **2008**, *33*, 3–19. [CrossRef]
6. Garuti, G.; Zaccarini, F.; Economou-Eliopoulos, M. Paragenesis and composition of laurite in chromitites of Othrys (Greece): Implication for Os-Ru fractionation in ophiolitic upper mantle of the Balkan peninsula. *Miner. Depos.* **1999**, *34*, 312–319. [CrossRef]
7. Garuti, G.; Zaccarini, F.; Moloshag, V.; Alimov, V. Platinum-Group minerals as indicator of sulfur fugacity in ophiolitic upper mantle: An example from chromitites of the Ray-Iz ultramafic complex (Polar Urals, Russia). *Can. Mineral.* **1999**, *37*, 1099–1115.
8. Kozlu, H.; Prichard, H.; Melker, F.; Fisher, P.; Brough, C.; Stueben, D. Platinum group element (PGE) mineralisation and chromite geochemistry in the Berit ophiolite (Elbistan/Kahramanmaraş), SE Turkey. *Ore Geol. Rev.* **2014**, *60*, 97–111. [CrossRef]
9. Prichard, H.M.; Neary, C.R.; Fisher, P.C.; O'Hara, M.J. Platinum group element (PGE) Ophiolite Complex, Saudi Arabia: An Example of Critical Mantle Melting to Extract and Concentrate PGE. *Econ. Geol.* **2014**, *103*, 1507–1529. [CrossRef]
10. Escayola, M.; Garuti, G.; Zaccarini, F.; Proenza, J.A.; Bedard, J.; Van Staal, C. Chromitite and platinum-group element mineralization at Middle Arm Brook, central Advocate ophiolite complex (Baie Verte peninsula, Newfoundland, Canada). *Can. Mineral.* **2011**, *49*, 1523–1547. [CrossRef]
11. Auge, T.; Legendre, O. Platinum-group element oxides from the Pirogues ophiolitic mineralization, New Caledonia; origin and significance. *Econ. Geol.* **1994**, *89*, 1454–1468. [CrossRef]
12. Auge, T.; Maurizot, P. Stratiform and alluvial platinum mineralization in the New Caledonia ophiolite complex. *Can. Mineral.* **1995**, *33*, 1023–1045.
13. Garuti, G.; Zaccarini, F. In-situ alteration of platinum-group minerals at low temperature: Evidence from chromitites of the Vourinos complex (Greece). *Can. Mineral.* **1997**, *35*, 611–626.
14. Kiseleva, O.N.; Zhmodik, S.M.; Damdinov, B.B.; Agafonov, L.V.; Belyanin, D.K. Composition and evolution of PGE mineralization in chromite ores from the Il'chir ophiolite complex (Ospa-Kitoi and Khara-Nur areas, East Sayan). *Russ. Geol. Geophys.* **2014**, *55*, 259–272. [CrossRef]
15. Grieco, G.; Bussolesi, M.; Eslami, A.; Gentile, A.; Cavallo, A.; Lian, D.; Yang, J.; Ghaseminejad, F. Differential platinum group elements (PGE) re-mobilization at low fS_2 in Abdasht and Soghan mafic-ultramafic complexes (Southern Iran). *Lithos* **2020**, *366–367*, 105523. [CrossRef]
16. Corrivaux, L.; LaFlamme, J.H.G. Minéralogie des éléments du groupe du platine dans les chromitites de l'ophiolite de Thetford Mines, Québec. *Can. Mineral.* **1990**, *28*, 579–595.
17. Gauthier, M.; Corrivaux, L.; Trottier, L.J.; Cabri, J.; Laflamme, J.H.G.; Bergeron, M. Chromitites platinifères des complexes ophiolitiques de l'Estrie–Beauce, Appalaches du Sud du Québec. *Miner. Depos.* **1990**, *25*, 169–178. [CrossRef]
18. Proenza, J.A.; Gervilla, F.; Melgarejo, J.C.; Vera, O.; Alfonso, P.; Fallick, A. Genesis of sulfide-rich chromite ores by the interaction between chromitite and pegmatitic olivine-norite dikes in the Potosí mine (Moa-Baracoa ophiolitic massif, eastern Cuba). *Miner. Depos.* **2001**, *36*, 658–669. [CrossRef]

19. Proenza, J.A.; Zaccarini, F.; Gervilla, F.; Melgarejo, J.C.; Garuti, G. Platinum Group Elements Mineralogy in Sulfide-Rich Chromitite from Potosí Mine (Moa-Baracoa Ophiolitic Massif, Eastern Cuba). In *Geosciences-Africa 2004*; Cardiff University: Cardiff, UK, 2004; Conference Abstracts; pp. 534–535.

20. Proenza, J.A.; Zaccarini, F.; Lewis, J.F.; Garuti, G.; Longo, F. Chromian spinel composition and the platinum-group minerals of the PGE-rich Loma Peguera chromitites, Loma Caribe peridotite, Dominican Republic. *Can. Mineral.* **2007**, *45*, 631–648. [CrossRef]

21. Pedersen, R.B.; Johannesen, G.M.; Boyd, R. Stratiform platinum-group element mineralizations in the ultramafic cumulates of the Leka ophiolite complex, central Norway. *Econ. Geol.* **1993**, *88*, 782–803. [CrossRef]

22. Prichard, H.M.; Ixer, R.A.; Lord, R.A.; Maynard, J.; Williams, N. Assemblages of platinum-group minerals and sulfides in silicate lithologies and chromite-rich rocks within the Shetland ophiolite. *Can. Mineral.* **1994**, *32*, 271–294.

23. Malitch, K.N.; Melcher, F.; Mühlhans, H. Palladium and gold mineralization in podiform chromitite at Kraubath, Austria. *Mineral. Petrol.* **2001**, *73*, 247–277. [CrossRef]

24. Çina, A.; Neziraj, A.; Karaj, N.; Johan, Z.; Ohnenstetter, M. PGE mineralization related to Albanian ophiolitic complex. *Geol. Carpat.* **2002**, *53*, 1–7.

25. Prichard, H.M.; Economou-Eliopoulos, M.; Fisher, P.C. Contrasting platinum-group mineral assemblages from two different podiform chromitite localities in the Pindos ophiolite complex, Greece. *Can. Mineral.* **2008**, *46*, 329–341. [CrossRef]

26. Kapsiotis, A.; Grammatikopoulos, T.A.; Tsikouras, V.; Hatzipanagiotou, K.; Zaccarini, F.; Garuti, G. Chromian spinel composition and platinum-group element (PGE) mineralogy of the chromitites from Milia area, Pindos ophiolite complex (NW Greece). *Can. Mineral.* **2009**, *47*, 1037–1056. [CrossRef]

27. Kiseleva, O.N.; Airiyants, E.V.; Belyanin, D.K.; Zhmodik, S.M. Podiform chromitites and PGE mineralization in the Ulan-Sar'dag ophiolite (East Sayan, Russia). *Minerals* **2020**, *10*, 141. [CrossRef]

28. Kiseleva, O.; Zhmodik, S. PGE mineralization and melt composition of chromitites in Proterozoic ophiolite complexes of Eastern Sayan, Southern Siberia. *Geosci. Front.* **2017**, *8*, 721–731. [CrossRef]

29. Bacuta, G.C., Jr.; Lipin, B.R.; Gibbs, A.K.; Kay, R.W. Platinum-group element abundance in chromite deposits of the Acoje ophiolite block, Zambales ophiolite complex, Philippines. In *Geo-Platinum Symposium Volume*; Prichard, H.M., Potts, P.J., Bowles, J.F.W., Cribb, S.J., Eds.; Elsevier: Amsterdam, The Netherlands, 1988; pp. 381–382.

30. Stumpfl, F.E.; Tarkian, M. Vincentite, a new palladium mineral from south-east Borneo. *Mineral. Mag.* **1974**, *39*, 525–527. [CrossRef]

31. Burgath, K.P. Platinum-group minerals in ophiolitic chromitites and alluvial placer deposits, Meratus-Bobaris area, southeast Kalimantan. In *Geo-Platinum Symposium Volume*; Prichard, H.M., Potts, P.J., Bowles, J.F.W., Cribb, S.J., Eds.; Elsevier: Amsterdam, The Netherlands, 1988; pp. 383–403.

32. Hattori, K.; Burgath, P.K.; Hart, S.R. Os-isotope study of platinum-group minerals in chromitites in Alpine-type ultramafic intrusions and the associated placers in Borneo. *Mineral. Mag.* **1992**, *56*, 157–164. [CrossRef]

33. Hattori, K.H.; Cabri, L.J.; Johanson, B.; Zientek, M.L. Origin of placer laurite from Borneo: Se and As contents, and S isotopic compositions. *Mineral. Mag.* **2004**, *68*, 353–368. [CrossRef]

34. Coggon, J.; Nowell, G.M.; Pearson, G.; Parman, S.W. Application of the 190Pt-186Os isotope system to dating platinum mineralization and ophiolite formation: An example from the Meratus mountains, Borneo. *Econ. Geol.* **2011**, *106*, 93–117. [CrossRef]

35. Zientek, M.L.; Pardiartob, B.; Simandjuntakb, H.R.W.; Wikramac, A.; Oscarsond, R.L.; Meiere, A.L.; Carlsone, R.R. Placer and lode platinum-group minerals in south Kalimantan, Indonesia: Evidence for derivation from Alaskan-type ultramafic intrusions. *Aust. J. Earth Sci.* **1992**, *39*, 405–417. [CrossRef]

36. Burgath, K.P.; Mohr, M. Chromitites and platinum-group minerals in the Meratus-Bobaris ophiolite zone southeast Borneo. In Proceedings of the Conference Metallogeny of Basic and Ultrabasic Rocks, Edinburgh, UK, 9–12 April 1985; IMM: London, UK, 1986; pp. 333–349.

37. Rustandi, E.; Nila, E.S.; Sanyoto, P.; Margono, U. *Geological Map of The Kotabaru Sheet, Kalimantan, Scale 1:250,000*; Geological Research and Development Centre: Bandung, Indonesia, 1995.

38. PT. SILO (Kotabaru Regency, Indonesia). Sebuku Iron Lateritic Ores. Geological Mapping of Sebuku Island, South Borneo. 2013; p. 85, Unpublished Internal Report. (In Indonesian)

39. Wijaya, I.G.N.K. Geology, Petrology and Geochemical of Chromite-PGM Deposits within the Ophiolite Complex in South Damar Area and its Vicinity. Bachelor's Thesis, Universitas Gadjah Mada, Sebuku Island, Indonesia, 2018; p. 221.

40. Imani, S.N.; Sihombing, F.M.H.; Indra, T.L.; Nugraheni, R.D. Characteristics of chromitite mineralization in Sebuku Island based on thin section, polished section, and geochemical data. *IOP Conf. Ser. Earth Environ. Sci.* **2020**, *538*, 012047. [CrossRef]

41. Stowe, C.W. Compositions and tectonic settings of chromite deposits through time. *Econ. Geol.* **1994**, *89*, 528–546. [CrossRef]

42. Arai, S. Chemistry of chromian spinel in volcanic rocks as a potential guide to magma chemistry. *Mineral. Mag.* **1992**, *56*, 173–184. [CrossRef]

43. Ferrario, A.; Garuti, G. Platinum-Group Minerals in Chromite-Rich Horizons in the Niquelandia Complex, (Central Goias, Brazil). In *Geo-Platinum Symposium Volume*; Prichard, H.M., Potts, P.J., Bowles, J.F.W., Cribb, S.J., Eds.; Elsevier Science Publishers: Amsterdam, The Netherlands; Springer: Dordrecht, The Netherlands, 1988; pp. 261–272.

44. Kamenetsky, V.S.; Crawford, A.J.; Meffre, S. Factors controlling chemistry of magmatic spinel: An empirical study of associated olivine, Cr-spinel and melt inclusions from primitive rocks. *J. Petrol.* **2001**, *42*, 655–671. [CrossRef]

45. Garuti, G.; Pushkarev, E.V.; Thalhammer, O.A.R.; Zaccarini, F. Chromitites of the Urals: Overview of chromite mineral chemistry and geo-tectonic setting (part 1). *Ofioliti* **2012**, *37*, 27–53.

46. Zaccarini, F.; Idrus, A.; Garuti, G. Chromite composition and accessory minerals in chromitites from Sulawesi, Indonesia: Their genetic significance. *Minerals* **2016**, *6*, 46. [CrossRef]

47. Idrus, A.; Septiana, S.; Zaccarini, F.; Garuti, G.; Hasria, H. Mineralogical, textural and chemical characteristics of ophiolitic chromitite and platinum group minerals from Kabaena Island (Indonesia): Their petrogenetic nature and geodynamic setting. *Minerals* **2022**, *12*, 516. [CrossRef]

48. Maurel, C.; Maurel, P. Étude experimental de la distribution de l'aluminium entre bain silicate basique et spinel chromifere. Implications pétrogenetiques: Tenore en chrome des spinelles. *Bull. Mineral.* **1982**, *105*, 197–202.

49. Rollinson, H. The geochemistry of mantle chromitites from the northern part of the Oman ophiolite: Inferred parental melt composition. Contrib. *Mineral. Petrol.* **2008**, *156*, 273–288. [CrossRef]

50. Evans, B.W.; Kuehner, S.M.; Joswiak, D.J.; Cressey, G. Serpentine, Iron-rich Phyllosilicates and Fayalite Produced by Hydration and Mg Depletion of Peridotite, Duluth Complex, Minnesota, USA. *J. Petrol.* **2017**, *58*, 495–512. [CrossRef]

51. Kranidiotis, P.; McLean, W.H. Systematic of chlorite alteration at the Phelps Dodge massive sulfide deposit, Matamagi, Quebec. *Econ. Geol.* **1987**, *82*, 1898–1911. [CrossRef]

52. Li, C.; Thakurta, J.; Ripley, E.M. Low-Ca contents and kink-banded textures are not unique to mantle olivine: Evidence from the Duke Island Complex, Alaska. *Mineral. Petrol.* **2012**, *104*, 147–153. [CrossRef]

53. Naldrett, A.J.; Duke, J.M. Platinum metals in magmatic sulfide ores. *Science* **1980**, *208*, 1417–1424. [CrossRef]

54. Garuti, G.; Zaccarini, F.; Cabella, R.; Fershtater, G. Occurrence of unknown Ru-Os-Ir-Fe oxides in the chromitites of the Nurali ultramafic complex, southern Urals, Russia. *Can. Mineral.* **1997**, *35*, 1431–1440.

55. Zaccarini, F.; Pushkarev, E.; Fershatater, G.; Garuti, G. Composition and mineralogy of PGE-rich chromitites in the Nurali lherzolite-gabbro complex, southern Urals. *Can. Mineral.* **2004**, *42*, 545–562. [CrossRef]

56. Zaccarini, F.; Proenza, J.A.; Rudashevsky, N.S.; Cabri, L.J.; Garuti, G.; Rudashevsky, V.N.; Melgarejo, J.C.; Lewis, J.F.; Longo, F.; Bakker, R.; et al. The Loma Peguera ophiolitic chromitite (Central Dominican Republic): A source of new platinum group minerals (PGM) species. *Neues Jahr. Mineral. Abhandl.* **2009**, *185*, 335–349. [CrossRef]

57. Uysal, I.; Zaccarini, F.; Sadiklar, M.B.; Bernhardt, H.J.M.; Bigi, S.; Garuti, G. Occurrence of rare Ru-Fe-Os-Ir-oxide and associated Platinum-group minerals (PGM) in the chromitite of Mugla ophiolite, SW-Turkey. *Neues Jahr. Mineral. Abhandl.* **2009**, *185*, 323–333. [CrossRef]

58. Bowles, J.F.W.; Suárez, S. The formation of alluvial platinum-group minerals: Present knowledge and the way ahead. *Mineral. Mag.* **2021**, *85*, 12–21. [CrossRef]

59. Zhou, M.-F.; Sun, M.; Keays, R.R.; Kerrich, R.W. Controls on platinum-group elemental distributions of podiform chromitites: A case study of high-Cr and high-Al chromitites from Chinese orogenic belts. *Geochim. Cosmochim. Acta* **1998**, 677–688. [CrossRef]

60. Boudier, F.; Al-Rajhi, A. Structural control on chromite deposits in ophiolites: The Oman case. In *Tectonic Evolution of the Oman Mountain*; Special Publications; Rollinson, H.R., Searle, M.P., Abbasi, I.A., Al-Lazki, A., Al Kindi, M.H., Eds.; The Geological Society of London: London, UK, 2014; Volume 392, pp. 259–273.

61. Nicolas, A.; Boudier, F. Textural insights on significance of ophiolitic chromitites, with special reference to Oman. *Acta Geol. Sin.* **2020**, *94*, 4. [CrossRef]

62. Melcher, F.; Grum, W.; Simon, G.; Thalhammer, T.V.; Stumpfl, E.F. Petrogenesis of the ophiolitic giant chromite deposits of Kempirsai, Kazakhstan: A study of solid and fluid inclusions in chromite. *J. Petrol.* **1997**, *38*, 1419–1458. [CrossRef]

63. Melcher, F.; Grum, W.; Thalhammer, T.V.; Thalhammer, O.A.R. The giant chromite deposits at Kempirsai, Urals: Constraints from trace element (PGE, REE) and isotope data. *Mineral. Depos.* **1999**, *34*, 250–272. [CrossRef]

64. Arai, S. Origin of podiform chromitites. *J. Asian Earth Sci.* **1997**, *15*, 303–310. [CrossRef]

65. Arai, S.; Miura, M. Formation and modification of chromitites in the mantle. *Lithos* **2016**, *264*, 277–295. [CrossRef]

66. Rollinson, H.R. Chromite in the mantle section of the Oman ophiolite: A new genetic model. *Isl. Arc* **2005**, *14*, 542–550. [CrossRef]

67. Uysal, I.; Tarkian, M.; Sadiklar, M.B.; Zaccarini, F.; Meisel, T.; Garuti, G.; Heidrich, S. Petrology of Al- and Cr-rich ophiolitic chromitites from the Muğla, SW Turkey: Implications from composition of chromite, solid inclusions of platinum-group mineral, silicate, and base-metal mineral, and Os-isotope geochemistry. *Contrib. Mineral. Petrol.* **2009**, *158*, 659–674. [CrossRef]

68. Baumgartner, R.J.; Zaccarini, F.; Garuti, G.; Thalhammer, O.A.R. Mineralogical and geochemical investigation of layered chromitites from the Bracco-Gabbro complex, Ligurian ophiolite, Italy. *Contrib Mineral. Petrol.* **2013**, *165*, 477–493. [CrossRef]

69. Arai, S.; Miura, M. Podiform chromitites do form beneath mid-ocean ridges. *Lithos* **2015**, *232*, 143–149. [CrossRef]

70. Llanes Castro, A.I.; Proenza, J.A.; Zaccarini, F.; Garuti, G.; Pacheco Sarlabous, M.S.C. Al- and Cr-rich chromitites from the Eastern Havana-Matanzas ophiolites (Western Cuba). *Episodes* **2015**, *38*, 334–343. [CrossRef]

71. Leblanc, M.; Nicolas, A. Ophiolitic chromitites. *Inter. Geol. Rev.* **1992**, *34*, 653–686. [CrossRef]

72. Zhou, M.-F.; Bai, W.-J. Chromite deposits in China and their origin. *Mineral. Depos.* **1992**, *27*, 192–199. [CrossRef]

73. Leblanc, M. Chromitite and ultramafic rock compositional zoning through a Paleotransform fault, Poum, New Caledonia. *Econ. Geol.* **1995**, *90*, 2028–2039. [CrossRef]

74. Zaccarini, F.; Garuti, G.; Proenza, J.A.; Campos, L.; Thalhammer, O.A.R.; Aiglsperger, T.; Lewis, J. Chromite and platinum-group-elements mineralization in the Santa Elena ophiolitic ultramafic nappe (Costa Rica): Geodynamic implications. *Geol. Acta* **2011**, *9*, 407–423.

75. Miura, M.; Arai, S.; Ahmed, A.H.; Mizukami, T.; Okuno, M.; Yamamoto, S. Podiform chromitite classification revisited: A comparison of discordant and concordant chromitite pods from Wadi Hilti, northern Oman ophiolite. *J. Asian Earth Sci.* **2012**, *59*, 52–615. [CrossRef]

76. Miura, M.; Arai, S.; Ahmed, A.H.; Tamura, A. Formation of discordant chromitite as the initiation of sub-arc mantle process: Observations from northern Oman ophiolite. *J. Mineral. Petrol. Sci.* **2014**, *109*, 38–43. [CrossRef]

77. Arai, S.; Abe, N. Podiform chromitite in the arc mantle: Chromitite xenoliths from the Takashima alkali basalt, Southwest Japan arc. *Mineral. Depos.* **1994**, *29*, 434–438. [CrossRef]

78. Çimen, O.; Toksoy-Köksal, F.; Öztüfekçi-Önal, A.; Aktağ, A. Depleted to refertilized mantle peridotites hosting chromitites within the Tunceli ophiolite, Eastern Anatolia (Turkey): Insights on the back arc origin. *Ofioliti* **2016**, *41*, 1–20.

79. Proenza, J.A.; Ortega-Gutiérrez, F.; Camprubí, A.; Tritlla, J.; Elías-Herrera, M.; Reyes-Salas, M. Paleozoic serpentinite-enclosed chromitites from Tehuitzingo (Acatlán Complex, southern Mexico): A petrological and mineralogical study. *J. S. Am. Earth Sci.* **2004**, *16*, 649–666. [CrossRef]

80. Chen, C.; Su, B.-X.; Xiao, Y.; Pang, K.-N.; Robinson, P.T.; Uysal, I.; Lin, W.; Qin, K.-Z.; Avcı, E.; Kapsiotis, A. Intermediate chromitite in Kızıldağ ophiolite (SE Turkey) formed during subduction initiation in Neo-Tethys. *Ore Geol. Rev.* **2019**, *104*, 88–100. [CrossRef]

81. Bussolesi, M.; Grieco, G.; Cavallo, A.; Zaccarini, F. Different Tectonic Evolution of Fast Cooling Ophiolite Mantles Recorded by Olivine-Spinel Geothermometry: Case Studies from Iballe (Albania) and Nea Roda (Greece). *Minerals* **2022**, *12*, 64. [CrossRef]

82. Zaccarini, F.; Bindi, L.; Garuti, G.; Proenza, J.A. Ruthenium and magnetite intergrowths from the Loma Peguera chromitite, Dominican Republic, and relevance to the debate over the existence of platinum-group element oxides and hydroxides. *Can. Mineral.* **2014**, *52*, 617–624. [CrossRef]

83. McDonald, A.M.; Proenza, J.A.; Zaccarini, F.; Rudashevsky, N.S.; Cabri, L.J.; Stanley, C.J.; Rudashevsky, V.N.; Melgarejo, J.C.; Lewis, J.F.; Longo, F.; et al. Garutiite, (Ni,Fe,Ir), a new hexagonal polymorph of native Ni from Loma Peguera, Dominican Republic. *Eur. J. Mineral.* **2010**, *22*, 293–304. [CrossRef]

84. Vyzmalová, A.; Laufer, F.; Drábek, M.; Stanley, C.; Bakker, R.J.; Bermejo, R.; Garuti, G.; Thalhammer, O.; Proenza, J.A.; Longo, F. Zaccariniite, RhNiAs, a new platinum-group mineral species from Loma Peguera, Dominican Republic. *Can. Mineral.* **2012**, *50*, 1321–1329.